

Detecting outlying demand in multi-leg bookings for transportation networks

Nicola RENNIE^{a,*}, Catherine CLEOPHAS^b, Adam M. SYKULSKI^c, and Florian DOST^{d,e}

^aSTOR-i Centre for Doctoral Training, Lancaster University, LA1 4YW, UK. (n.rennie@lancaster.ac.uk)

^bInstitute for Business, Christian-Albrechts-University Kiel, Kiel, Germany. (cleophas@bwl.uni-kiel.de)

^cDept. of Mathematics and Statistics, Lancaster University, LA1 4YF, UK. (a.sykulski@lancaster.ac.uk)

^dInstitute of Business and Economics, Brandenburg University of Technology, 03046 Cottbus, Germany. (florian.dost@b-tu.de)

*Corresponding Author: Nicola Rennie (n.rennie@lancaster.ac.uk)

Abstract

Planners require accurate demand forecasts when optimising offers to maximise revenue on network products, such as railway itineraries. However, network effects complicate demand forecasting in general and outlier detection in particular. For example, sudden increases in demand for a specific destination in a transportation network not only affect legs arriving at that destination, but also their feeder legs. Network effects are particularly relevant when transport service providers, such as railway or coach companies, offer many multi-leg itineraries. In this paper, we present a novel method for generating automated ranked outlier lists to support analysts in adjusting demand forecasts. To that end, we propose a two-step method for detecting outlying demand from transportation network bookings. The first step clusters network legs to appropriately partition and pool booking patterns. The second step identifies outliers within each cluster and creates a ranked alert list of affected legs. We show that this method outperforms analyses that independently consider leg data without regard for network implications, especially in highly-connected networks where most passengers book multi-leg itineraries. A simulation study demonstrates the robustness of the approach and quantifies the potential revenue benefits from adjusting network demand forecasts for offer optimisation. Finally, we illustrate the applicability on empirical data obtained from Deutsche Bahn.

Keywords: Analytics; Forecasting; Outlier detection; Clustering; Network revenue management.

1 Introduction and State of the Art

Transport service providers such as railways (Yuan et al., 2018) or long-distance coach services (Augustin et al., 2014) offer a large number of interconnected legs that let passengers travel along a multitude of itineraries. Such services require providers to solve a variety of related planning problems, ranging from service network design to demand forecasting and offer optimisation across the network.

Revenue management (RM) through offer optimisation is a particularly relevant example of a network planning problem that depends on accurate demand forecasts. Specifically, the concept entails controlling the set of offered fare classes such that, given predicted demand for the offers, the expected revenue is maximal. For railways, this translates to optimising the set of offered fare classes per travel itinerary, while accounting for the expected demand for this itinerary and for those itineraries that require seats on mutual legs. Klein et al. (2020) review how single-leg practices to RM generalise to the network setting. Weatherford (2016) surveys RM forecasting methods and particularly considers itinerary-level forecasting for airlines. Further contributions, e.g. Weatherford and Belobaba (2002) and Rennie et al. (2021), demonstrate the negative effects of inaccurate demand forecasts on revenue performance, but neglect network effects.

Our research focuses on detecting demand outliers in a network setting. Here, we define an outlier as a booking pattern observed on a leg across a booking horizon that resulted from short-term systematic changes in demand in one or several related itineraries. A *leg* describes a direct connection between two stops in a transport network, whereas an *itinerary* is any combination of legs that can be jointly booked as one travel product. We term a unit sold as a *booking*, and the accumulation of bookings across the booking horizon as a *booking pattern*. Booking patterns may be reported per leg or per itinerary.

Network effects challenge outlier detection in two ways: On the one hand, demand outliers on the itinerary level affect multiple legs included in the itinerary. On the other hand, such outliers may not be recognisable given noise from other overlapping itineraries when considering leg bookings in isolation. As a result, directly extracting outliers from an entire network of booking data is likely to be an intractable problem in most realistic sized networks. Therefore, to support firms in identifying outliers in such networks, we propose a methodological solution which (i) clusters legs of a network, (ii) detects joint leg demand outliers within each cluster, and (iii) compiles ranked alert lists of affected legs. We show that our methodology significantly improves the performance of outlier detection in a network setting, contributing to several related streams of inquiry.

In the RM domain, little existing research examines how to account for demand outliers. For historical hotel booking data, Weatherford and Kimes (2003) discuss a simple method of removing observations that are more than $\pm 3\sigma$ away from the mean. Rennie et al. (2021) apply functional analysis to detect outliers on individual legs. Neither, however, consider outliers affecting multiple legs of a network, leaving this challenge as an open problem.

Outside the RM domain, Barrow and Kourentzes (2018) propose a functional approach for outlier detection in call arrival forecasting, also without regard for network effects. General outlier detection in networks often focuses on identifying outlying parts of the network. Fawzy et al. (2013) use this approach in wireless sensor networks to find faulty nodes. Ranshous et al. (2015) provide an overview of the extension to identifying

outlying nodes when the network changes over time. Most research on dynamic networks concentrate on analysing a single time series connected to each node, rather than analysing a set of time series, as required when booking patterns are reported for multiple departures. Hyndman et al. (2016) note that the problem of identifying unusual time series (within a collection of similar time series) is not as extensively studied as other outlier detection problems. We implement the approach suggested by Hyndman et al. (2016) to identify outlying time series based on principal component analysis (PCA), as a benchmark to our newly proposed approach.

We suggest to aggregate and analyse booking patterns from *legs* as opposed to *itineraries* based on two considerations. First, when a large network features many possible itineraries, each individual itinerary only receives a small number of bookings on average, challenging any data analysis. Secondly, when offering a large number of potential itineraries, providers rarely store all booking patterns on an itinerary level. For example, capacity-based RM as described in Strauss et al. (2018) frequently considers booking patterns on the leg level to ensure the availability of capacity on each leg of a requested itinerary. Accordingly, the methodology proposed here is compatible with capacity-based RM.

The first part of our methodological approach clusters legs in a network. We propose to do this by measuring the similarity of booking patterns observed on different legs via functional dynamical correlation (Dubin and Müller, 2005). We choose this measure for its freedom from restrictive assumptions, but other correlation measures could be used to the same end in a modular approach. Accordingly, we shall benchmark different correlation measures in Appendix C.1.

The second part of our methodological approach detects outliers from booking patterns within each cluster to form a ranked alert list. In the literature, focus is often restricted to binary outlier detection without regard for quantifying how critical an outlier is. However, practical network RM often relies on manual forecast adjustments (Currie and Rowley, 2010; Schütze et al., 2020). Previous research has shown that the resulting judgemental forecasts can be biased and even superfluous (Lawrence et al., 2006; De Baets and Harvey, 2020). To avoid such collateral damages, we use extreme value theory to contribute a ranked alert list of affected departures to help analysts identify the need for further analysis and adjustments. In the context of this paper, we use the term *departure* to indicate a journey that leaves the origin station at a unique time and date.

Perera et al. (2019) note that such forecasting support tools can improve user judgement by reducing complexity for the analyst. Analysts' time is limited and they are unlikely to have the time to investigate every departure which is flagged as an outlier. For example, Deutsche Bahn experts estimate that they can reasonably adjust less than 1% of forecasts. This motivates us to focus analysts' attention by constructing a ranked alert list. We consider an outlier as more critical if it indicates a larger demand shift and if it is identified across multiple legs. Finally, in contrast to the single-leg case discussed

in Rennie et al. (2021), analysts have several choices of network forecast adjustment. The best choice of forecast adjustment is not obvious, and we further quantify the impact on revenue of different potential adjustments in a simulation study.

In summary, this paper contributes (i) a method for identifying network legs that will benefit from joint outlier detection; (ii) a method to aggregate outlier detection across any number of legs to create a ranked alert list; (iii) wide-ranging simulation studies to test the method’s performance against various benchmarks, evaluated in terms of outlier classification performance, and then potential revenue improvements from forecast adjustments; and (iv) demonstrates applicability on empirical railway booking data from Deutsche Bahn.

2 Method

In journeying across transportation networks, a common set of passengers traverses certain legs. Therefore, certain legs share common outliers, as, for example, a sudden increase in demand from passengers travelling from one end of the network to attend an event at the other end would cause a sudden increase in demand for each of the legs in-between. Neither considering each leg independently, nor jointly considering the network as a whole, will create the best results when a network spans multiple regions that differ strongly in expected demand. This raises the question of which legs to consider jointly for outlier detection.

Therefore, in Section 2.1 we propose a method to *cluster* legs such that (i) legs in the same cluster share common outliers and can be considered jointly for outlier detection, and (ii) legs in different clusters experience independent demand outliers and should be considered separately. Subsequently, in Section 2.2, we suggest a method for analysing bookings within a cluster of similar legs. Based on this, we propose a method to rank identified outliers by severity.

2.1 Clustering legs using correlation-based minimum spanning trees

To cluster legs based on correlations in observed bookings, we first consider the network as a graph where nodes represent the stations and edges represent the legs of a journey. We illustrate this on the simple network shown in Figure 1a. In this example, two train lines (red and blue) intersect at two stations (B and C). The red train arrives at stations B and C before the blue train, which creates two possible transfer connections for passengers: (i) switch from red to blue at B, (ii) switch from red to blue at C. Transfers from the blue to red train are not feasible.

Common graph clustering algorithms, as exemplified in Schaeffer (2007), seek to cluster the nodes of the graph. In contrast, we wish to cluster similar legs, which correspond to edges in the original graph 1a. Hence, we invert the graph to make existing clustering

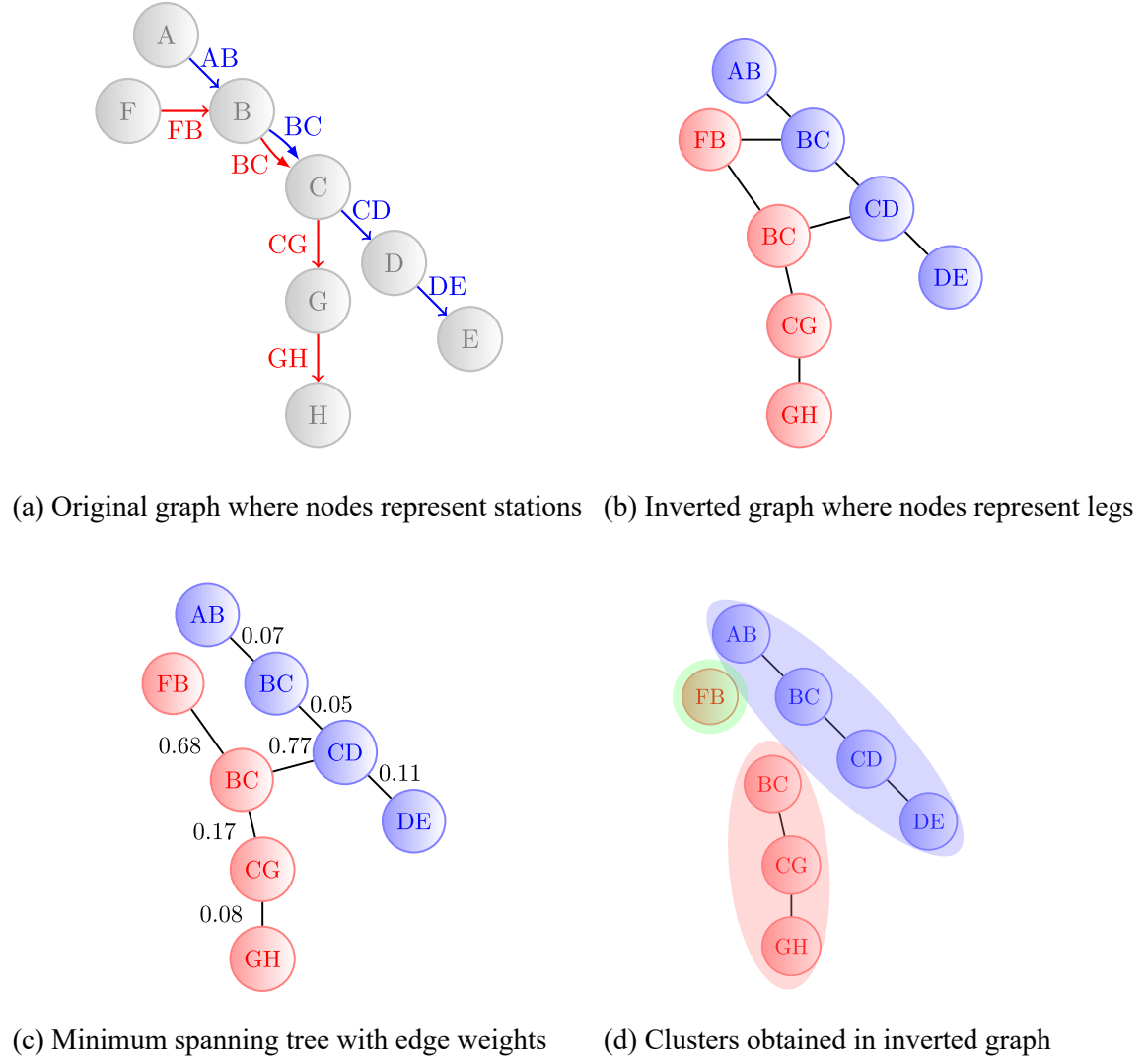


Figure 1: Correlation-based minimum spanning tree clustering

algorithms applicable. In this inversion (Figure 1b), the directed edges become nodes, e.g. the edge from A to B becomes node AB. The inverted graph features an undirected edge between two nodes (two legs of the original graph) when:

- both legs are in the same train line and share a common station, e.g. legs CD and DE are connected through station D, or
- the legs are in different train lines but share a common transfer station where a connection is possible, e.g. leg FB (red line) and BC (blue line) are connected through station B. However, AB (blue line) and BC (red line) would not be connected by an edge as no connection can be made between them (as we have assumed the red train arrives at B and C before the blue train).

In theory, this transformation could also create edges between legs that share a common entry or exit node, e.g. FB (red line) and AB (blue line), or CG (red line) and CD (blue line). Given that such pairs of legs would never occur in the same itinerary, no itinerary forecast adjustment would apply to both legs. Therefore, including an edge between them, potentially allowing them to be in the same cluster and receive a joint forecast adjustment, is counter-intuitive. In addition, in exploratory analysis of the empirical data, we found that correlations between these types of legs were very low across the entire network section considered.

The algorithm aims to assign those legs that experience *similar bookings* to the same cluster and those that experience *dissimilar bookings* to separate clusters. A corresponding metric only needs to consider similarity between adjacent legs, which share a connecting station, since edges do not exist in the inverted graph otherwise. We propose to quantify this similarity via the correlation between booking patterns.

Calculating correlations between booking patterns We compute the functional dynamical correlation (Dubin and Müller, 2005). Functional dynamical correlation is based on the calculation of scalar products between pairs of smoothed booking patterns – see Appendix A.1 for details. We use the average of these paired correlations over time as the measure of similarity between two legs. Unlike more common statistical correlation measures, such as Pearson correlation, functional dynamical correlation does not assume a specific type of relationship between variables (e.g. linearity). It also accounts for the time dependency between observations within the booking horizon, when the length of intervals between observations varies. For example, in much empirical RM data, as described in Section 3, the time between observations decreases as the departure date approaches. Further, alternative measures for calculating correlations from functional data (such as functional canonical correlation) often make restrictive assumptions, which real data does not fulfil (He et al., 2003). In Appendix C.1, we benchmark the clustering algorithm under different correlation measures.

Transforming correlation measures into edge weights To represent the relationship between legs in the network, i.e. the nodes in the inverted graph, we attach weights to the edges in the inverted graph. These weights are interpreted as distances: a higher edge weight indicates that the connected nodes are more dissimilar. Therefore, an applicable weight function should be non-negative. Further, the weight function needs to ensure that any negatively correlated legs are marked as more dissimilar. Even though negative correlation may imply that outlier demand jointly affects both legs, we expect it to affect negatively correlated legs in different ways. Therefore, these would require different adjustments and should be in different clusters. To satisfy these requirements

we shall define the edge weights as:

$$w_{(ij,jk)} = 1 - \rho(ij, jk), \quad (1)$$

where $\rho(ij, jk)$ is the correlation between bookings on legs ij and jk .

Clustering network legs We recommend a minimum spanning tree (MST) algorithm to allow for clusters of irregular shapes. For example, in Figure 1b, a cluster may include AB and DE because they are in the same line, rather than clustering AB and FB. Minimum spanning tree approaches work well for clusters with irregular boundaries (Zahn, 1971). MST-based clustering approaches also do not assume that clusters are of similar sizes (Peter and Victor, 2010). This makes them particularly suitable for railway networks constructed as a series of interlocking lines, where the points of intersection are often not equally spaced. MST-based approaches have previously been used in optimising layouts of railway networks (Liang et al., 2020). Alternative clustering approaches (such as k -means), often assume a specific shape of clusters (spherical, for k -means).

A *spanning tree* of a graph is a subgraph that includes all vertices in the original graph and a minimum number of edges, such that the spanning tree is connected. Then, the MST is the spanning tree with the minimum summed edge weights – see Figure 1c. Since the inverted graph is weighted, we use Prim’s algorithm (Prim, 1957) to calculate the MST – see Appendix A.2 for a detailed introduction. Any one-to-one transformation of the weight function, $w_{(ij,jk)}$ will produce an identical minimum spanning tree.

There are two approaches to obtaining clusters from an MST: (i) pre-defining the number of clusters as k , and removing the $k - 1$ edges with highest weight; or (ii) setting a threshold for the edge weights and remove all edges with weights above some threshold, creating an emergent number of clusters. We implement the threshold-based approach, as this ensures that each cluster has the same minimum level of correlation. In contrast, setting the number of clusters in advance could result in very heterogeneous levels of correlation across clusters. Further, setting k too low may result in legs with dissimilar features being grouped together. We apply a threshold correlation of 0.5 – the level at which legs are more correlated than they are not. This corresponds to a transformed edge weight of 0.5. In the example given in Figure 1c, this means removing all legs with a weight above 0.5, resulting in the three clusters shown in Figure 1d.

Note that the outlier detection procedure described next applies to individual clusters, but does not require a particular clustering approach. Hence, alternative approaches, as reviewed in Schaeffer (2007), could be utilised. In particular, in applications to other transport services, such as airline networks, alternative clustering algorithms may be more appropriate. The choice of which clustering algorithm is most appropriate should be driven by the network topology. The choice of an MST-based approach, which often returns linear clusters, is appropriate for the railway data considered here, given the

linear nature of the underlying network structure. The performance of MST clustering algorithms in this application is evaluated in Appendix C.1.

It is, of course, reasonable to suggest that an edge-based clustering be applied instead of the graph inversion and node-based clustering presented here. Literature on edge-based clustering is far more limited, and the aim of such approaches tends to be in improving the visualisation of networks with a very high number of edges by reducing the number of edge crossings Qu et al. (2007), rather than in grouping together the most similar edges. In contrast, the inversion and node-based approach aims to cluster together network legs that exhibit the highest degree of similarity. However, we acknowledge that, alongside these advantages, there may be some drawbacks. The main disadvantage of the node-based approach lies in the need to decide on criteria to select edges to include in the inverted graph. In this paper, which focuses on the application to railway networks, the criteria were based on domain expertise and knowledge of how resulting forecast adjustments could be made. In other contexts, different criteria may be more appropriate and some human input would be required to ensure the correct choices are made.

2.2 Detecting outliers in clusters of legs

Given established clusters, we propose to identify demand outliers within each cluster and to quantify their severity to provide a *ranked alert list* of departures. The previously described clustering allows for processing the outlier detection in parallel for separate clusters, enabling efficient computing.

To identify which departures to include in the alert list, we consider the *functional depth* of their booking patterns. This step could also rely on other measures of exceedance, including univariate “threshold” approaches, which look at aggregated bookings and ignore the distribution of bookings over time. We propose to rely on functional depth, as previous work has found this to be the most effective as an outlier detection mechanism (Rennie et al., 2021).

To compute the functional depth, consider N departures, observed over L legs. Let $\mathbf{y}_{nl} = (y_{nl}(t_1), \dots, y_{nl}(t_T))$ be the booking pattern for the n^{th} departure on leg l , observed over T booking intervals t_1, \dots, t_T . Let \mathcal{Y}_l be the set of N booking patterns for leg l . For each leg and departure, calculate the functional depth given the related booking patterns – see Appendix A.3 and Hubert et al. (2012) for technical details.

For each leg l , we calculate a threshold for the functional depth using the approach of Febrero et al. (2008). This method (i) resamples the booking patterns with probability proportional to their functional depths (such that any outlying patterns are less likely to be resampled), (ii) smooths the resampled patterns, and (iii) sets the threshold C_l as the median of the 1^{st} percentiles of the functional depths of the resampled patterns. Here, we use the 1^{st} percentile of the depths as the default threshold, as this has been found to work well in practice (Febrero et al., 2008; Rennie et al., 2021). Appendix C.2.2

explores alternative threshold choices. Booking patterns with a functional depth below the threshold C_l are classed as outliers.

To create ranked alert lists, we first define z_{nl} to be the normalised difference between the functional depth and the threshold:

$$z_{nl} = \frac{C_l - d_{nl}}{C_l}. \quad (2)$$

This transforms the depth measure d_{nl} into a measure of *threshold exceedance*. Values of z_{nl} greater than zero relate to booking patterns classified as outliers. Normalising by the threshold, C_l , ensures the values of z_{nl} are comparable between different legs.

Next, we define the sums of threshold exceedances across legs:

$$z_n = \sum_{l=1}^L z_{nl} \mathbb{1}_{\{z_{nl} > 0\}}. \quad (3)$$

We sum only those values of z_{nl} that are greater than zero to avoid outliers being masked when they occur only in a subset of legs. This sum implicitly accounts for both the size of an outlier – larger outliers further exceeding the threshold, resulting in larger values of z_{nl} – and for the number of legs where a departure is classified as an outlier (by summing a larger number of non-zero values). To provide an example, Figure 2 shows those values of z_n that exceed zero for a four leg section of the Deutsche Bahn network as discussed further in Section 3.2. These values of z_n correspond to departures where the booking pattern for *at least* one leg is identified as an outlier, whereas all other departures have no detected outliers in any leg such that $z_n = 0$.

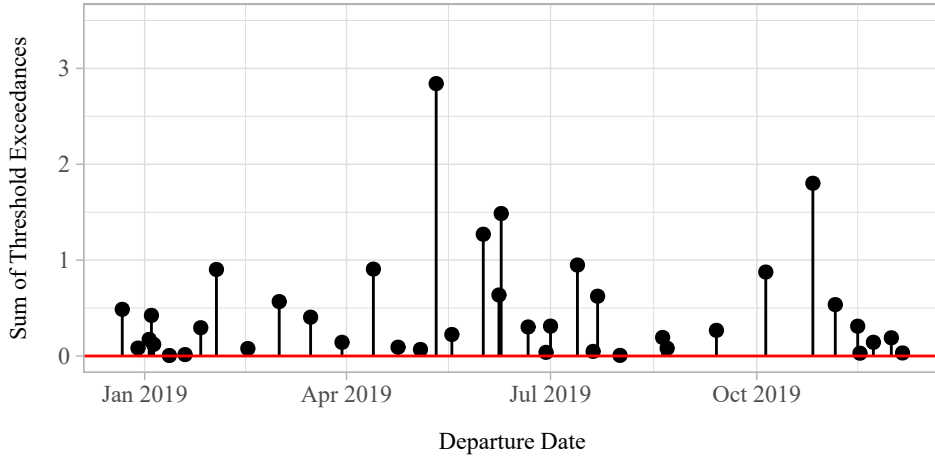


Figure 2: z_n as defined in equation (3) for a four leg section of the Deutsche Bahn network

To create a ranked list of outlier departures, i.e. those with a non-zero sum of threshold exceedances, we assign a severity θ_n . A higher value of θ_n indicates the departure is more likely to be affected by extreme outlier demand, and hence should be targeted first by RM analysts.

To model threshold exceedances, we turn to extreme value theory (EVT) – a branch of statistics that deals with modelling rare events that occur in the tails of the distribution. Given that outliers are unusual events, which occur in the tails of distributions, EVT is a clear direction to turn to for modelling outliers – see Talagala et al. (2019). There are two common approaches to EVT: (i) block maxima, which examines the maximum value in evenly-spaced blocks of time, e.g. annual maxima, and (ii) peaks over threshold, which examines all observations that exceed some threshold (Leadbetter, 1991). The generalised Pareto distribution (GPD) is commonly used to model the tails of distributions in the peaks over threshold approach (Pickands, 1975). Motivated thus, we fit a generalised Pareto distribution (GPD) to the sum of threshold exceedances given in equation (3). The GPD has three parameters with probability density function:

$$f(x|\mu, \sigma, \xi) = \frac{1}{\sigma} \left(1 + \frac{\xi(x - \mu)}{\sigma} \right)^{(-\frac{1}{\xi} - 1)}, \quad (4)$$

for

$$x \in \begin{cases} [\mu, \infty) & \xi \geq 0 \\ [\mu, \mu - \frac{\sigma}{\xi}] & \xi < 0. \end{cases} \quad (5)$$

Here, μ specifies the location, σ the scale, and ξ the shape of the distribution. We fit the parameters using maximum likelihood estimation (Grimshaw, 1993) via the R package POT (Ribatet and Dutang, 2019). A kernel density estimate of the empirical distribution of $z_n > 0$ from Figure 2 is shown in Figure 3a. The resulting fitted GPD is shown in Figure 3b. The GPD fit appears to be reasonable compared to the empirical distribution; further analysis in Appendix D.5 supports this.

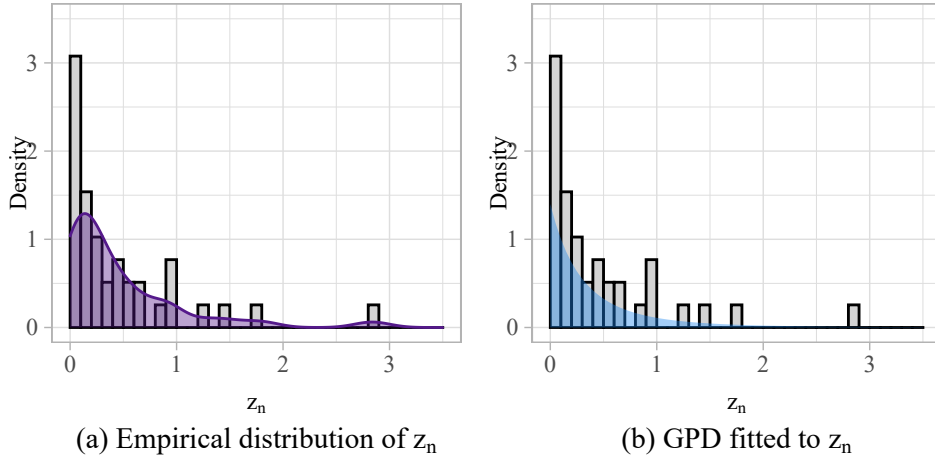


Figure 3: Distribution of z_n values from Figure 2

Two common issues arise in fitting GPDs: (i) the choice of threshold and (ii) the independence of the data points. When the threshold is too low, the assumption of a GPD no longer holds; when it is too high, there are too few data points to fit. We select a

threshold of 0, i.e. we fit the GPD to values of $z_n > 0$. Rather than change the threshold at GPD level, we control the number of observations the GPD is fitted to by varying the percentile used for the individual leg thresholds, C_l . We choose C_l as suggested by Febrero et al. (2008), and find that this choice works well and provides sufficient outlying points to fit a GPD both in simulated and empirical data.

To account for the second issue, applications of extreme value theory frequently first *decluster* the peaks over the threshold to ensure independence between observations (Fawcett and Walshaw, 2007). To that end, the analysis may only consider the maximum of two peaks that occur within some small time window. For transport departures, it is theoretically possible that observed outliers may be dependent; e.g. increased demand caused by Easter not only affects Easter Sunday but also the surrounding days. However, similar outliers may also result from independent events. As we aim to identify outlying departures rather than the underlying events, this argument causes us not to decluster here.

We define θ_n as the non-exceedance probability given by the CDF of the GPD:

$$\theta_n = F_{(\mu, \sigma, \xi)}(z_n) = \begin{cases} 1 - \left(1 + \frac{\xi(z_n - \mu)}{\sigma}\right)^{-\frac{1}{\xi}} & \xi \neq 0 \\ 1 - \exp\left(-\frac{(z_n - \mu)}{\sigma}\right) & \xi = 0 \end{cases} \quad (6)$$

Formally, θ_n is the probability that, given an outlier occurs, the sum of threshold exceedances is at least as large as z_n . Thus, it is *not* the probability that a departure is an outlier. However, we use this non-exceedance probability as a measure of outlier *severity* on a scale of 0 to 1.

Departures with functional depths that do not fall below the threshold on any legs carry a severity of zero, i.e. they are classified as regular departures. It is conceivable to estimate the uncertainty of θ_n (Smith, 1985) to determine further levels of criticality, e.g. if there are several departures with the same outlier severity, the one with smallest uncertainty would be ranked first. However, given the continuous nature of the data, it is unlikely that multiple departures carry an identical severity. Hence, we leave uncertainty estimation to future research.

From the severity defined in equation (6), we construct a *ranked alert list* containing all departures with a non-zero outlier severity. Although functional depth could be directly used to construct the ranked alert list, computing the severity provides a measure of the difference between ranks and is more easily interpreted by analysts. The top 8 ranked outliers relating to Figure 2, are shown in Table 1.

In practice, RM analysts' time and resources allow them to examine and adjust controls or forecasts only for a limited number of suspicious booking patterns. Those departures which (i) exceed the functional depth threshold in only one leg or (ii) exceed the threshold only to a small degree have lower but strictly non-zero severity. These outliers are most likely false positives and potentially waste analysts' time. Hence, we suggest

| Ranking | Departure | Severity | Legs with $z_{nl} > 0$ |
|----------|------------|----------|------------------------|
| 1 | 11/05/2019 | 0.985 | AB, BC, CD, DE |
| 2 | 26/10/2019 | 0.960 | AB, BC, CD, DE |
| 3 | 09/06/2019 | 0.942 | AB, BC, CD, DE |
| 4 | 01/06/2019 | 0.922 | AB, BC, CD, DE |
| 5 | 13/07/2019 | 0.874 | AB, BC, CD, DE |
| 6 | 13/04/2019 | 0.865 | CD, DE |
| 7 | 02/02/2019 | 0.864 | CD, DE |
| 8 | 05/10/2019 | 0.857 | AB, BC, CD, DE |
| \vdots | \vdots | \vdots | \vdots |

Table 1: Ranked alert list for cluster = $\{AB, BC, CD, DE\}$

limiting the length of the list in practice.

To limit the length of the alert list, we might (i) only include departures if their severity is above some threshold, or (ii) set a maximum length. Since we wish to control the number of alerts an analyst will receive, we analyse outlier detection performance with respect to the maximum length of the alert list. Recall that we classify departures as outliers if and only if their outlier severity exceeds zero. Therefore, if the required length of the alert list exceeds the number of identified outliers, we do not include further departures. Appendix C.2.7 presents further results on the performance of the outlier detection when varying the outlier severity threshold.

3 Empirical Study

To demonstrate the practical applicability of the proposed clustering and outlier detection, we apply it to a set of empirical data obtained from Deutsche Bahn. The Deutsche Bahn long-distance network consists of over 1,000 train stations, letting the provider offer more than 110,000 direct origin-destination combinations. The numbers grow further when accounting for alternative transfer itineraries and for multiple departures per day. Figure 4 shows the empirical distribution of the number of legs included in itineraries that passengers booked in November 2019. Only 7% of passengers booked single-leg itineraries, whereas almost half of all booked itineraries span five or more legs.

3.1 Clustering legs in the Deutsche Bahn network

28 leg study First, we consider a section of the Deutsche Bahn railway network that consists of two intersecting train lines over a total of 27 stations and 28 legs – see Figure 5. The red train arrives at the connecting stations before the blue train. Hence, the network offers three transfer connections: changing from red to blue at either Fulda,

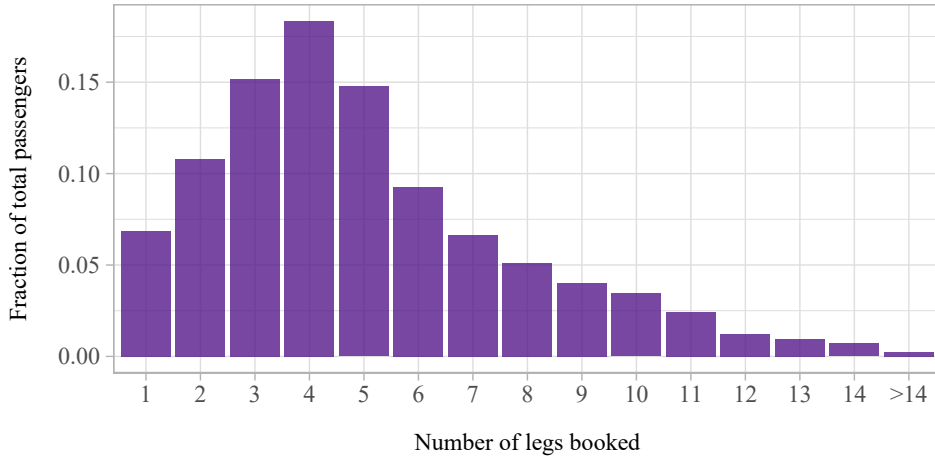


Figure 4: Distribution of number of legs per booked itinerary from Deutsche Bahn data

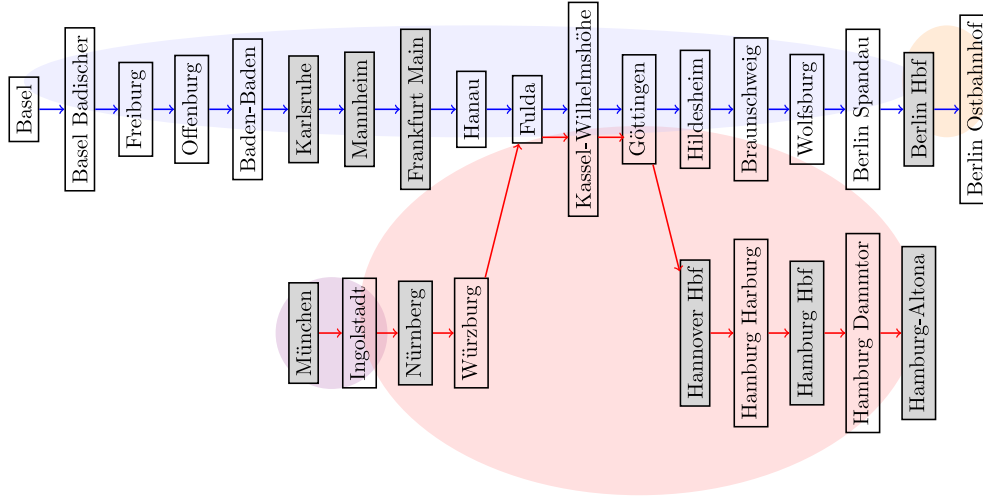
Kassel-Wilhelmshöhe, or Göttingen. This creates 240 potential travel itineraries. For each leg in this network section, Deutsche Bahn records 359 booking patterns for departures between December 2018 and December 2019. Each booking pattern ranges over 19 booking intervals; the first observation occurs 91 days before departure.

We firstly apply the correlation-based clustering approach of Section 2.1, using a threshold of 0.5, such that only legs with a minimum correlation of 0.5 can be in the same cluster. In Figure 5a, coloured bubbles indicate the four resulting clusters: Each train line splits into one large and one small cluster.

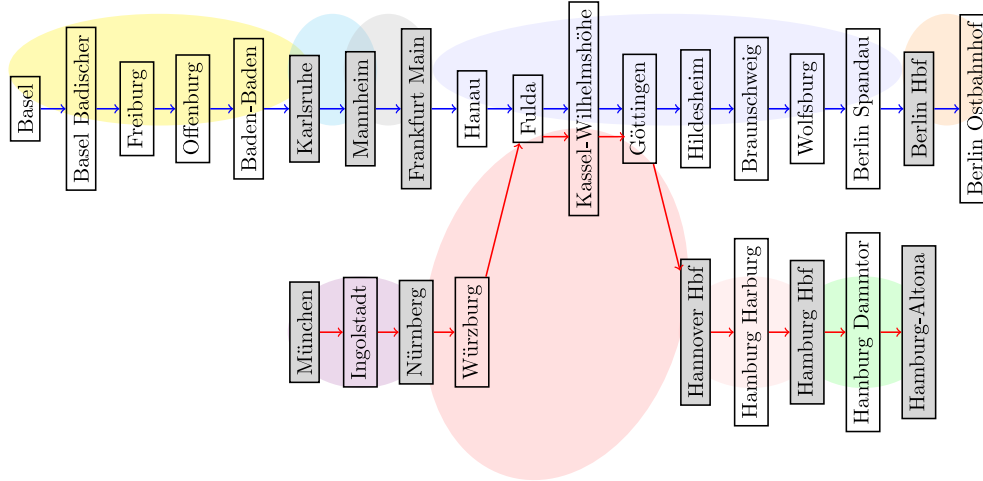
To evaluate clustering on empirical data, where the true underlying demand for each itinerary is unknown, we use the network topology to check whether resulting clusters are plausible. To that end, we propose the following set of rules:

- Different train lines must belong to different clusters. Even when passengers can transfer between lines, we expect relatively few passengers to make the same connection. Further, for forecasting and analyst interventions, it makes sense to consider train lines separately.
- Train lines are further split into different clusters on either side of a major station. As many passengers leave the train at a major station and many *different* passengers board, we shall assume a relatively small proportion of passengers book itineraries that pass a major station. Similarly, given that itinerary demand share is driven by which journeys are most common, and passengers often either board or alight at a major station, it is intuitive to have a cluster that contains the legs between major stations.

Deutsche Bahn assigns an ordinal indicator of importance to each station, ranging from 1 to 7. We define a *major station* to be in *Category 1*. The entire Deutsche Bahn network includes 21 major stations, where the considered network section includes nine



(a) Correlation-based clustering, $\rho \geq 0.5$



(b) Rule-based cluster

Figure 5: Comparison of correlation-based and rule-based clustering of Deutsche Bahn network

major stations. Figure 5b highlights major stations in grey and shows the clusters resulting from the rules listed above.

The correlation-based clustering returns four clusters, whereas the rule-based clustering returns nine clusters. Nevertheless, the resulting clusters share similar features. Firstly, the two distinct train lines end up in different clusters in either approach. For legs in distinct train lines, correlation tends to be higher between legs that share a transfer station, but not to a convincing extent – correlation is at most 0.22. A correlation threshold of 0.27 creates two clusters (one for each train line). Secondly, the break points

for the correlation-based approach are a subset of the break points, i.e. major stations, in the rule-based approach. We conclude that the correlation-based approach achieves similar results as the rule-based approach without requiring expert input.

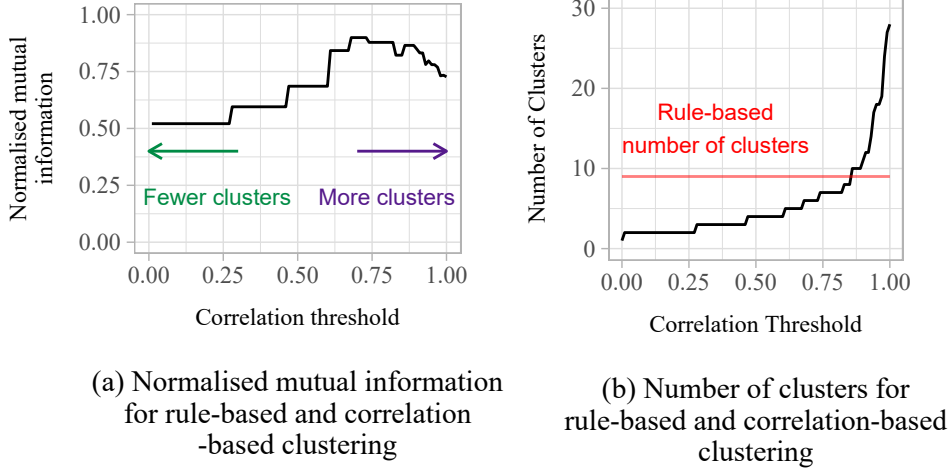


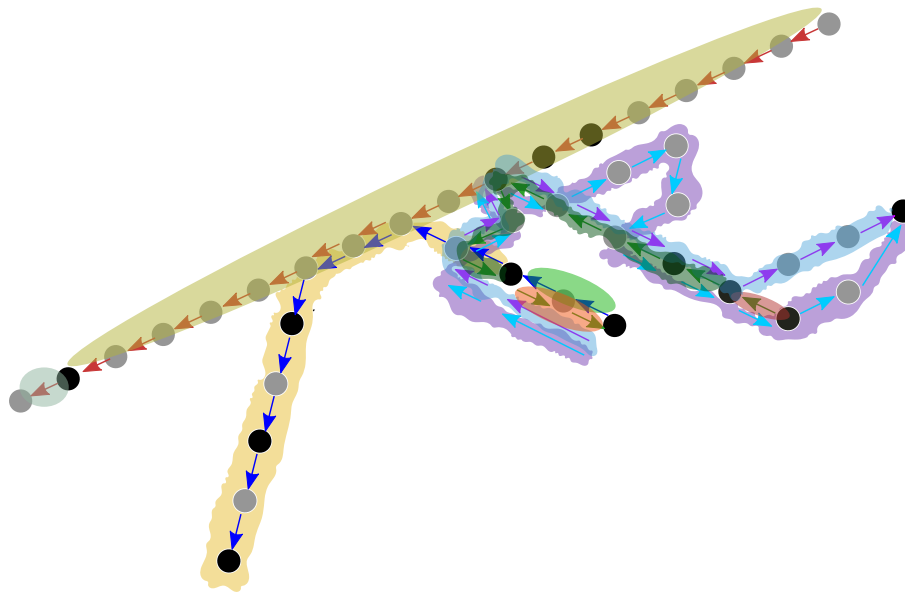
Figure 6: Comparison of rule-based and correlation-based clustering in a two line railway network

We can formally compare clustering results using the **Normalised Mutual Information (NMI)** (Amelio and Pizzuti, 2015). The NMI is 1 if two clusterings are identical, and 0 if they are completely different (see Appendix A.4 for details). Figure 6a shows the NMI between the correlation- and rule-based approaches while varying the threshold in the correlation-based approach from 0 to 1. This shows that both approaches achieve similar results, with an NMI reaching 0.899. The approaches are generally more similar at higher correlation thresholds (around 0.7), since the rule-based approach generally creates more clusters. Figure 6b compares the number of clusters of the two approaches – as the correlation threshold changes, the number of clusters ranges from 1 (everything in a single cluster) to 28 (each leg in its own cluster), demonstrating the flexibility of the correlation-based approach.

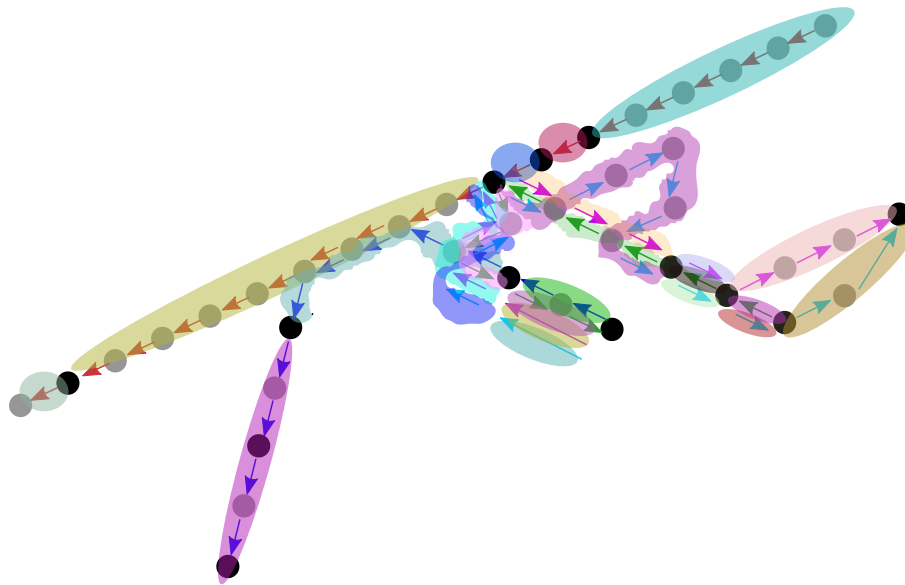
63 leg study We extend the empirical study to five train lines to further demonstrate the complexity that considering the network structure brings to clustering and outlier detection. The five line network consists of 40 stations, with 63 legs. As seen in Figure 7, there are often multiple train lines which cover the same leg, or may travel in the opposite direction. As the larger size of the network makes visualisation more difficult, in Figure 7 stations are represented by circles, with major stations highlighted in black.

Figure 7(a) shows the results of the correlation-based clustering with a default threshold $\rho = 0.5$. This results in 9 clusters, with two train lines each forming their own cluster containing all legs. The break points of the clusters occur at major stations, as also previously seen for two train lines. The pattern of breaking clusters at major stations

persists as the correlation threshold is varied. In comparison, the output of the rule-based clustering shown in Figure 7(b) results in 24 clusters, with many being of size 1.



(a) Correlation-based clustering, resulting in 9 clusters with breakpoints occurring at major stations



(b) Rule-based clustering for a five line network, resulting in 24 clusters

Figure 7: Comparison of rule-based and correlation-based clustering in a five line railway network

In these empirical studies, we applied rule-based clustering only to evaluate the plausibility of the results from correlation-based clustering. We do not advocate for it as a method in itself. A rule-based approach, where the clusters are based on domain experts’ categorisations, would not be able to respond to the evolving importance of stations across different train lines and departure times. Notably, the correlation-based method is not simply a data-driven method for uncovering major stations, but rather for identifying legs where multi-leg itineraries cause similar booking patterns, and thus could change and adapt over time. We further evaluate clustering performance in a simulation study, where the itinerary-level demand is known, in Appendix C.1. The results in the remainder of the paper rely on correlation-based clustering.

3.2 Detecting outliers in the Deutsche Bahn data

Having established clusters, we apply outlier detection independently to each cluster. To exemplify this on empirical data, we apply the outlier detection procedure to a representative four-leg cluster from the Deutsche Bahn network. Applying the proposed outlier detection approach on empirical data cannot precisely judge detection accuracy, given there is no labelled data on genuine outliers. However, this analysis demonstrates the full process of outlier detection on empirical data including, e.g. seasonality and underlines practical implications.

For this analysis, we consider a cluster of four legs from the Deutsche Bahn network with stations anonymised and denoted by A, B, C, D, and E. This cluster results from applying the correlation-based clustering to a new section of the Deutsche Bahn network to Figure 5.

Figure 8 shows the booking patterns for each of the four legs; bookings are scaled to be between 0 and 1. From initial visual inspection, the structure of the booking patterns appears similar, with some obvious outliers appearing across multiple legs.

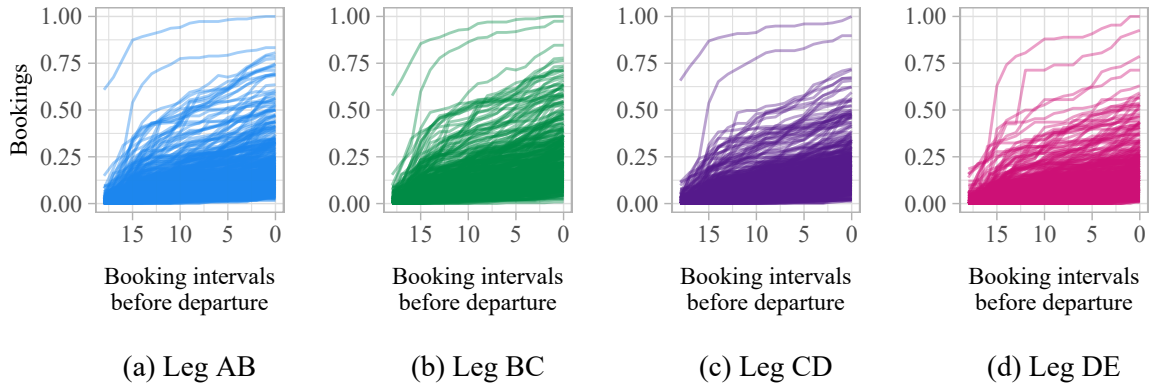


Figure 8: Booking patterns for each leg

To pre-process the data for outlier detection, we transform the booking patterns by applying a functional regression model (Ramsay and Silverman, 1997). We then apply

the outlier detection to the residual booking patterns. In this pre-processing, we correct for three factors: (i) departure day of the week; (ii) departure month of the year; and (iii) the length of the booking horizon.¹

The functional regression fits a mean function to the booking patterns for each different factor in the model. Table 9 in Appendix D.1 compares models including different factors. Let $y_{nl}(t)$ be the n^{th} booking pattern for leg l . Then:

$$\begin{aligned}
y_{nl}(t) = & \beta_{0l}(t) + \beta_{1l}(t)\mathbb{1}_{Mon_{nl}} + \beta_{2l}(t)\mathbb{1}_{Tue_{nl}} + \beta_{3l}(t)\mathbb{1}_{Wed_{nl}} + \\
& \underbrace{\beta_{4l}(t)\mathbb{1}_{Thu_{nl}} + \beta_{5l}(t)\mathbb{1}_{Fri_{nl}} + \beta_{6l}(t)\mathbb{1}_{Sat_{nl}}}_{\text{Departure Day of the Week}} + \\
& \beta_{7l}(t)\mathbb{1}_{Jan_{nl}} + \beta_{8l}(t)\mathbb{1}_{Feb_{nl}} + \beta_{9l}(t)\mathbb{1}_{Mar_{nl}} + \\
& \beta_{10l}(t)\mathbb{1}_{Apr_{nl}} + \beta_{11l}(t)\mathbb{1}_{May_{nl}} + \beta_{12l}(t)\mathbb{1}_{Jun_{nl}} + \beta_{13l}(t)\mathbb{1}_{Jul_{nl}} + \\
& \underbrace{\beta_{14l}(t)\mathbb{1}_{Aug_{nl}} + \beta_{15l}(t)\mathbb{1}_{Sep_{nl}} + \beta_{16l}(t)\mathbb{1}_{Oct_{nl}} + \beta_{17l}(t)\mathbb{1}_{Nov_{nl}}}_{\text{Departure Month of the Year}} + \\
& \underbrace{\beta_{18l}(t)\mathbb{1}_{Shorter Horizon_{nl}}}_{\text{Length of Booking Horizon}} + e_{nl}(t).
\end{aligned} \tag{7}$$

where, e.g. $\mathbb{1}_{Mon_{nl}} = 1$ if departure n relates to a Monday, 0 otherwise. In this model, $\beta_{0l}(t)$ represents the average bookings for Sunday departures in December, with a regular length of booking horizon, and $\beta_{pl}(t)$ for $p > 0$ represent deviations from this mean pattern. The $\beta_{pl}(t)$ are functions of time, which allows for relationships between factors to evolve over the booking horizon. Given that functional depths are calculated independently for each leg, we apply the regression model independently for each leg. The resulting residuals are shown in Appendix D.2, Figure 33.

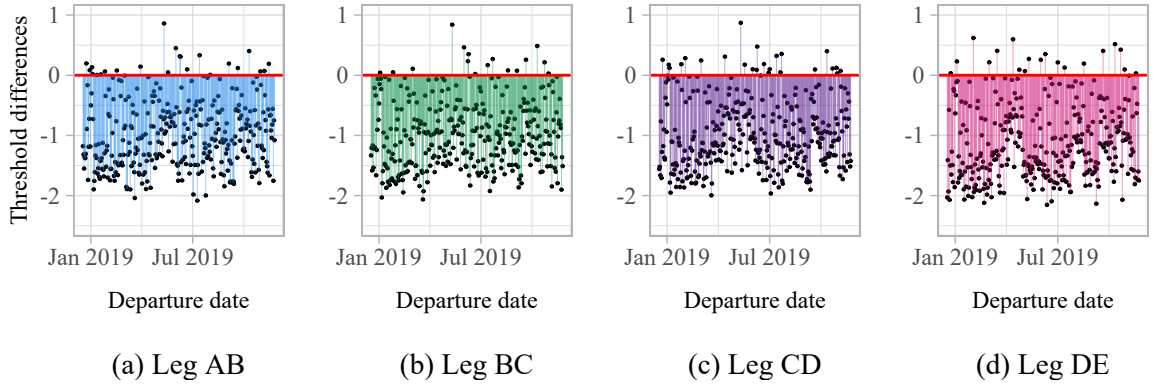


Figure 9: Threshold exceedances per leg, z_{nl}

Functional regression preserves the correlation between different legs, as verified in Appendix D.7, Table 11b. The clustering approach can consider either the correlations

¹Deutsche Bahn offer a regular booking horizon of 6 months, with the first observation of bookings occurring around 3 months before departure. Due to schedule changes, shorter booking horizons of 3 months apply for departures from mid-December to mid-March.

between the booking patterns or the residual booking patterns. Given that the functional depths (the basis for the outlier detection) are calculated on the residuals, we suggest using correlation between residual patterns to define the clusters. For this data set, the same clusters resulted in either case.

We calculate the functional depth of each booking pattern and compute the threshold as described in Section 2.2. We then transform the depths as per equation (2) to obtain z_{nl} , as shown in Figure 9. The sums of threshold exceedances, z_n , were shown earlier in Figure 2, with the empirical distribution and fitted generalised Pareto distribution shown in Figures 3a and 3b, respectively.

Figure 10 highlights the outliers detected in each leg in pink, while depicting outliers detected in other legs but *not* in that leg in blue. Regular patterns are grey.

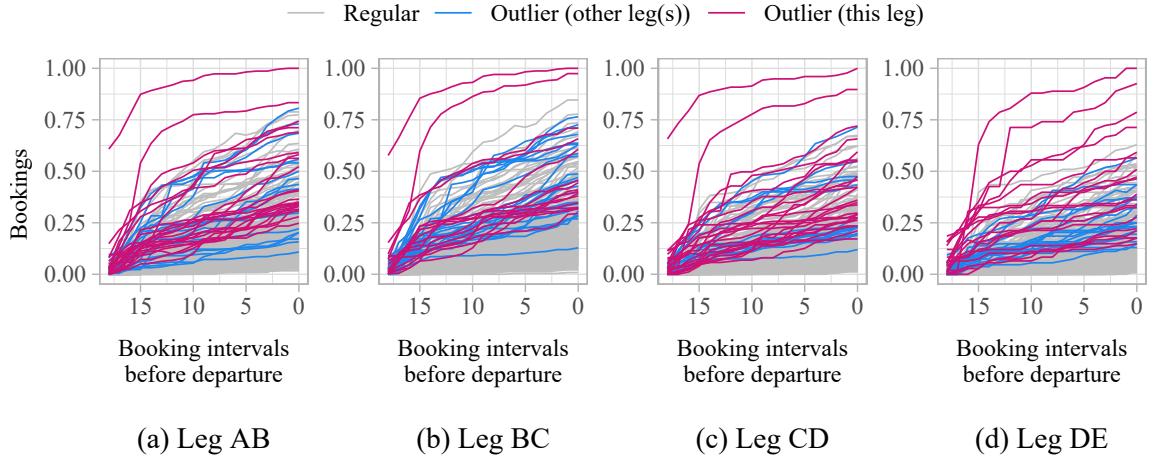


Figure 10: Outliers detected in booking patterns

Of the 40 outliers (11% of departures) detected across all legs, 23 outliers (almost 60%) could be attributed to known events or holidays. When considering only the top 10 outliers, the percentage rose to 70%. A further departure detected as an outlier had been previously flagged by Deutsche Bahn. The firm implemented a booking stop to control sales on that departure for multiple connected legs. Appendix D.6 provides further details on the distribution of identified outliers across legs.

4 Simulation Study: Outlier Detection Performance

We first implement a simulation study to evaluate the outlier detection performance given known outliers. By varying demand for itineraries in one cluster, we create outliers that are observable on both the leg and network level.

The simulation models a network consisting of 5 stations and 4 legs, as shown in Figure 11, mirroring the structure of an empirical railway network cutout. The network includes 10 possible itineraries represented by $\mathcal{O} = \{AB, AC, AD, AE, BC, BD, BE, CD, CE, DE\}$.

On each itinerary, the firm offers seven fare classes. In this model, a fare class describes a particular price or fare that is associated when booking a ticket to travel the itinerary in that class. There are no additional restrictions differentiating classes. We consider differentiated demand from two customer types represented by the set $\mathcal{I} = \{1, 2\}$.

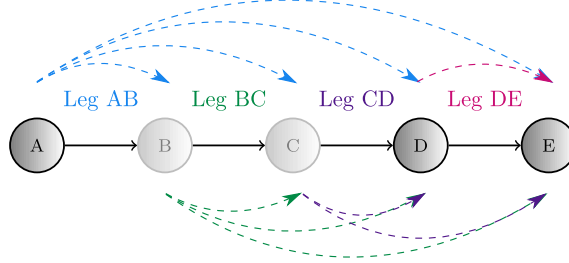


Figure 11: Four-leg-cluster, dotted lines indicate 10 possible itineraries

4.1 Demand settings

The simulation generates booking requests per customer type i according to a non-homogeneous Poisson process, where the arrival rate per itinerary o , $\lambda_{i,o}(t)$, at time t , is given by:

$$\lambda_{i,o}(t)|(D_o = d_o) = d_o \times \phi_{io} \frac{t^{a_{io}-1}(1-t)^{b_{io}-1}}{B(a_{io}, b_{io})}. \quad (8)$$

Here, ϕ_{io} is the fraction of customers of type i and $D_o \sim \text{Gamma}(\alpha_o, \beta_o)$ with probability density function:

$$f(d_o|\alpha_o, \beta_o) = \frac{\beta_o^{\alpha_o}}{\Gamma(\alpha_o) d_o^{\alpha_o-1} e^{\beta_o d_o}}. \quad (9)$$

We generate demand over a horizon of 3,600 time slices to ensure $\lambda_{i,o}(t) < 1$. This level of detail is required to accurately parameterise the dynamic program for bid price control. The resulting bookings are aggregated into 18 booking intervals.

We assume that customers book the cheapest available fare class and differ in price-sensitivity. We define p_{ijo} as the probability that a customer of type i pays up to fare class j on itinerary o . Combining this demand model with the given network creates 210 demand parameters. Appendix B.3, Table 2 lists all parameter values. We set the parameters to mirror common RM assumptions (Weatherford and Bodily, 1992): (i) valuable customers from type 1 book later than customers from type 2, (ii) customers book earlier for longer journeys, and (iii) customers are willing to pay a higher fare class if they are travelling further. The majority of passengers book tickets boarding at A and leaving at E; this ensures the correlation between the legs exceeds 0.5 and guarantees that the legs are correctly modelled in the same cluster. As detailed in Appendix D.7, we validated that the functional dynamical correlation between the four legs for simulated data is comparable to empirical railway data. Appendix D.7 also compares the simulated

and empirical booking patterns to validate parameter choices. We generate all regular demand based on these parameters.

The simulation excludes trend and seasonality to evaluate outlier detection approaches in a best-case-scenario. In other words, if an algorithm fails on observations from stationary demand, it will likely not perform better given more demand variability.

4.2 Outlier generation and evaluation

We generate demand volume outliers by changing the parameters of the Gamma distribution that governs the level of total demand according to equations (8) and (9). Previous work found the proportion of outliers had little effect on outlier detection performance in the single-leg case (Rennie et al., 2021). Therefore, we generate booking patterns for 500 departures per demand setting, with 1% of departures experiencing outlier demand. That is, we generate 495 departures from the regular demand distribution, and 5 outliers from a set of twelve outlier distributions where the mean has shifted by $\pm 10\%$, $\pm 20\%$, $\pm 30\%$, $\pm 40\%$, $\pm 50\%$, and $\pm 60\%$. For every shift in mean, we reduce the variance of the outlier demand distribution by 80%. This still results in an overall increase in variance of total demand in the presence of outliers, but also ensures that we sample sufficiently outlying demand values.

We differentiate outlier scenarios in terms of the affected network components. Firstly, we evaluate a scenario where outlier demand affects all network itineraries. We consider the case where each outlier is randomly drawn from one of the twelve outlier distributions, resulting in outliers from a mixture of different distributions. This lets us test whether the ranking of the alert list mirrors the outliers' underlying degree of demand deviation. Then, we consider each of the twelve outlier distributions in isolation to assess the sensitivity of detection. Secondly, we evaluate a scenario where outliers only affect a single itinerary. This evaluates the benefits of clustering multiple legs. Appendix C.2.6 considers the practically relevant case of outliers affecting a subset of itineraries. The full extent of simulation experiments is shown in Appendix B.3.1.

Each combination of outcomes can be classified into one of four categories: (i) assigning a non-zero outlier severity to a genuine outlier creates a true positive (TP); (ii) assigning a zero outlier severity to a regular observation creates a true negative (TN); (iii) assigning a non-zero outlier severity to a regular observation creates a false positive (FP); (iv) assigning a zero outlier severity to a genuine outlier creates a false negative (FN). This classification enables us to compute the true positive rate (TPR) for the top R ranked departures in the alert list:

$$TPR_R = \frac{TP_R}{TP + FN}, \quad (10)$$

where TP_R is the number of true positives in the top R departures. The true positive rate lies between 0 and 1, where 1 means all genuine outliers were identified. We evaluate performance across 1,000 stochastic simulations.

In an ideal setting, the alert list should feature, from top to bottom, large outliers and subsequently smaller outliers. Therefore, we also use the distribution of outliers within the ranked alert list to evaluate how well the method ranks the most critical outliers.

4.3 Benchmarked outlier detection approaches

For benchmarking, we term the newly proposed approach FD+Agg and compare it to two alternatives from the literature: Principal Component Analysis combined with High Density Regions (PCA + HDR) as inspired by Hyndman et al. (2016), and the leg-based functional depth analysis as proposed in Rennie et al. (2021).

Comparison with PCA + HDR: This benchmark (i) computes features (e.g. mean, variance, curvature) of the booking patterns for the total demand in a cluster; (ii) uses PCA (Yang and Shahabi, 2004) to identify the first two principle components from the features; and (iii) uses HDR, a density based approach (Hyndman, 1996), to find the ν points with lowest density in the first two principal components. These points are classified as outliers. Extended details of the method, including the list of features, can be found in Appendix B.2. This method provides an ordering of the outliers but not a severity measure, as illustrated by Figure 12.

Comparison with non-ranked, single-leg approaches: To highlight to critical features of FD-Agg, we benchmark (i) the use of severity measures to rank outliers and (ii) the inclusion of network effects. To isolate the effects of each of these features, we perform two separate benchmark tests:

We evaluate the effect of ranking outliers by measuring the increase in precision when ranking outliers. For example, we consider the precision in the top 5 ranked departures, versus 5 randomly chosen departures with non-zero outlier probabilities (i.e., as in Rennie et al. (2021)). The change in precision when considering the top R departures, $\Delta(Precision)_R$, is given by:

$$\Delta(Precision)_R = \frac{TP_R}{TP_R + FP_R} - \frac{TP_{R(random)}}{TP_{R(random)} + FP_{R(random)}}, \quad (11)$$

where $TP_{R(random)}$ is the number of true positives in a random selection of R departures with non-zero severity, and $FP_{R(random)}$ is defined analogously for false positives.

We quantify the value of accounting for network effects by computing ranked alert lists for each leg in isolation. We then compare the true positive rates to the aggregated, network-driven approach presented in this paper.

4.4 Experimental results on detecting outliers in multiple legs

As a first experiment, we consider the scenario where outlier demand equally affects all itineraries and legs within the cluster. For this scenario, Figure 12a illustrates how the

true positive rate (TPR) increases when ranking outliers for different lengths of the alert list. The red line indicates the number of genuine outliers. The true positive rates for our method (denoted as FD+Agg) are promising, with a TPR of around 0.2 for a list length of 1. Since there are five genuine outliers, this indicates that a genuine outlier is almost always ranked top. Results under different functional depth thresholds are found in Appendix C.2.2.

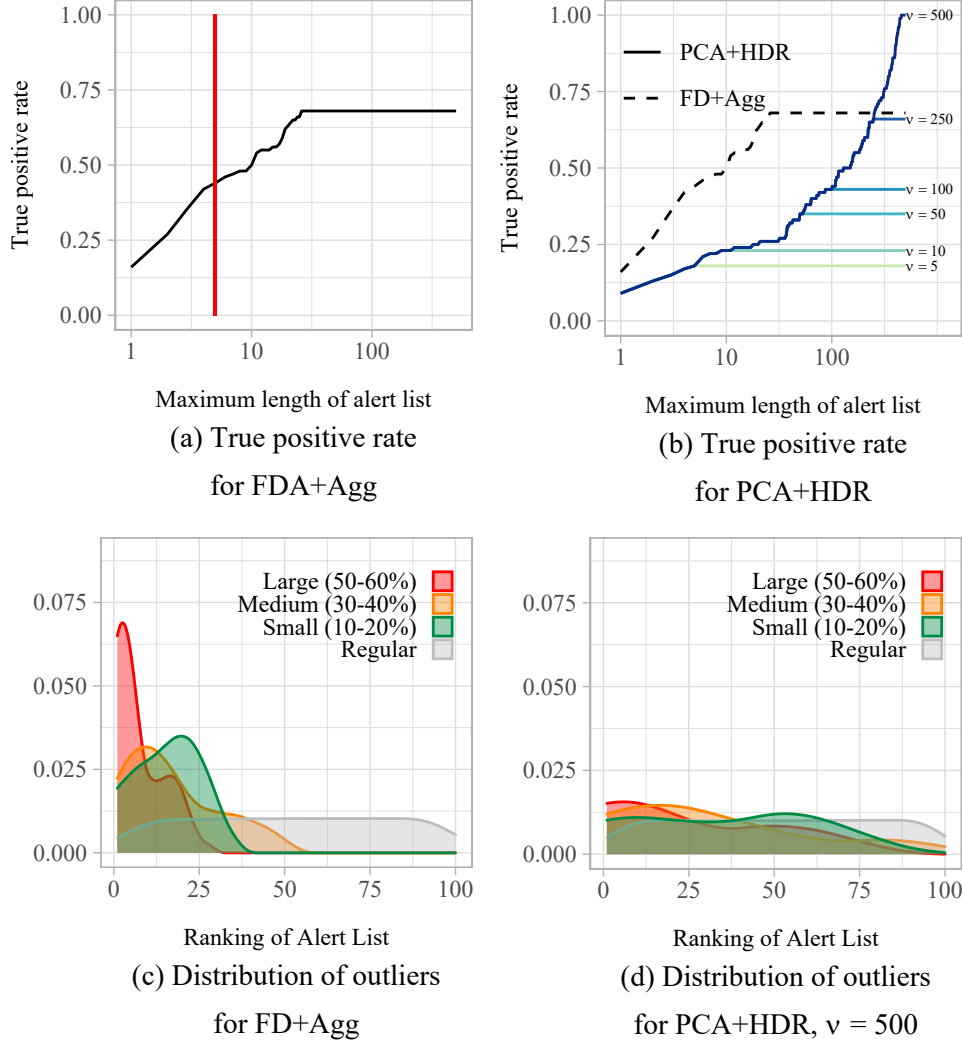


Figure 12: Performance and benchmark comparison with PCA+HDR for demand-volume outliers in all itineraries, showing improved performance

PCA+HDR benchmark results. The PCA+HDR approach requires a given number of outliers to detect, ν , as input. Therefore, we compare the performance of the benchmark method under different choices of ν to FD+Agg.

Figure 12b shows that the true positive rate achieved by FD+Agg consistently exceeds that achieved by PCA+HDR. In order to achieve the same level of true positive rate,

PCA+HDR would need to classify around 250 departures (i.e. 50%) as outliers. In comparison, FD+Agg achieves this rate from about 30 classified outliers on. We consider this a successful validation of the effect of ranking outliers in FD+Agg. These results are displayed in tabular format in Appendix C.2.1.

Figure 12c shows the distribution of each magnitude of outlier in the alert lists. Under FD+Agg, the modes of the distributions generally fall where they should, as larger outliers are ranked higher. The smaller variance in the ranking of the larger magnitude outliers indicates that they are easier to detect. The higher variance of the medium sized outliers can be explained as the ranking of a medium sized outlier is dependent on which other types of outliers occur: if there is a large and a medium outlier, the medium outlier is ranked lower; if there is a small and a medium outlier, the medium outlier is ranked higher. The distribution of outliers detected by PCA+HDR, shown in Figure 12d, also has the modes in the correct order. However, there is much more overlap between the distributions, showing its inability to correctly rank the outliers.

Comparison with non-ranked approach. Figure 13a highlights how the precision improves when ranking outliers as opposed to listing them in random order. Ranking particularly improves precision when the alert list covers only a small number of departures. As domain experts indicate that analysts cannot target more than 1% of departures, ranking focuses resources and thereby provides large benefits in practice. Nevertheless, Figure 13a (when contrasted with Figure 12a) also highlights the trade-off between reducing the number of false alerts and identifying all outliers. A shorter length of alert list increases precision, but reduces the true positive rate.

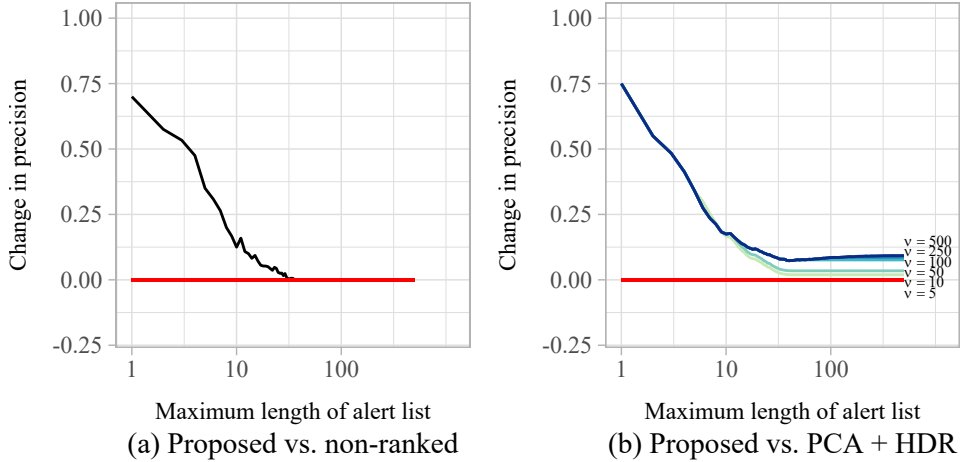


Figure 13: Change in precision from ranking detected outliers in FD+Agg as dependent on the length of the alert list

The increase in precision from applying our method compared to PCA+HDR is similar to the increase in precision from the inclusion of the ranking (see Figure 13b). This

suggests that PCA+HDR performs reasonably well in terms of outlier detection, but poorly in terms of ranking the outliers.

Comparison with single-leg approach. Figure 14 shows the true positive rate when a ranked alert list is computed for each leg in isolation versus in the proposed aggregated manner. Here, we consider outlier demand generated by a 50% increase in the affected legs as an illustrative example. We analyse detection performance by breaking down results in terms of which itinerary the outlier demand is generated in. We show only the results relating to itineraries AB, AC, AD, and AE. Figure 26 in Appendix C.2.5 details results for the further itineraries yielding similar conclusions. For results when outlier demand is generated across combinations of itineraries, see Appendix C.2.6.

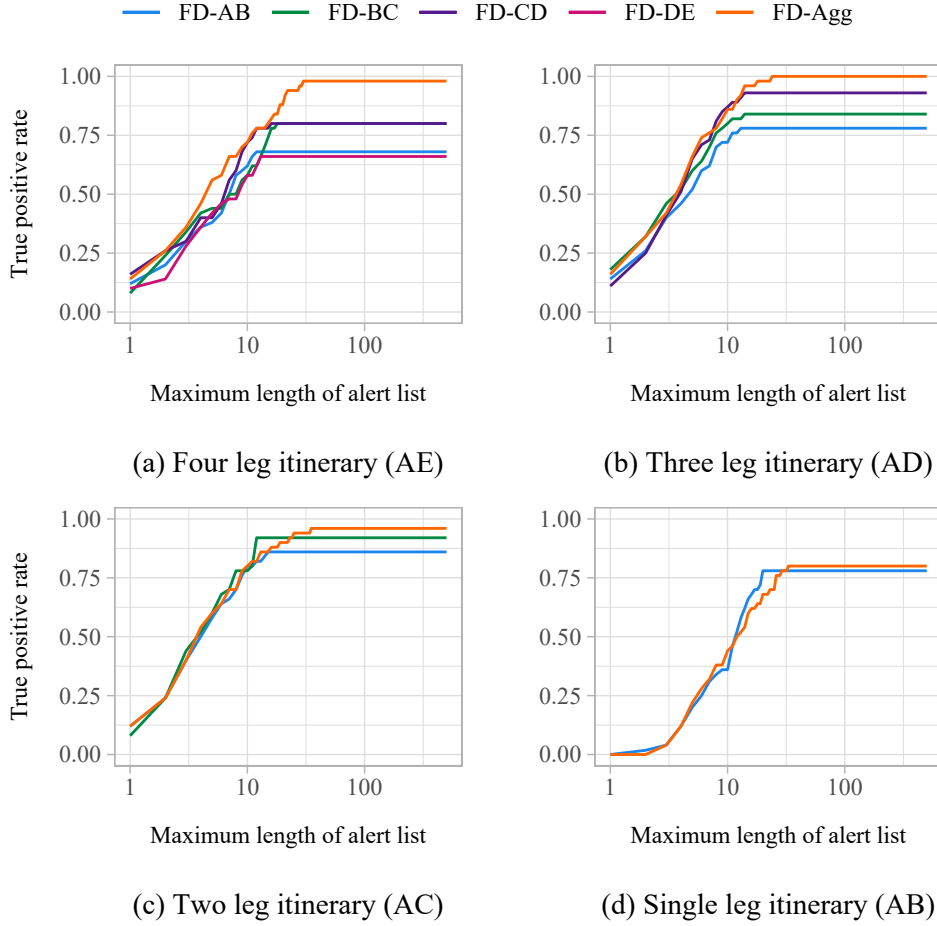


Figure 14: True positive rate for single itinerary outliers when applying FD+Agg versus detection on isolated legs

In all cases, the true positive rate for clusters is higher than in any of the individual legs. This is because when considering the leg's bookings in isolation under outlier demand that affects multiple legs, the noise from other itineraries prevents detecting the outlier

in every leg. However, clustering increases the number of detected genuine outliers.

Aggregation is most beneficial when the outlier demand affects the most legs. In our example, this applies when itinerary AE experiences outlier demand, as shown in Figure 14a. The lower true positive rates in legs AB and DE result as different combinations of itineraries also utilise these legs. The aggregation is less beneficial when outlier demand affects an itinerary consisting of only one or two legs, since we aggregate the analysis across legs that are actually not affected by outlier demand. However, there is a modest gain in true positive rate even in this case – compare Figure 14(c). This is due to the knock-on effects of decreased capacity on the affected legs, impacting the bid prices for any itineraries which include these legs. For some lengths of alert list, the leg-level true positive rates are higher than the aggregated approach, due to false positives from unaffected legs being included in the list. However, even for itinerary AB (Figure 14d), where false positives from unaffected legs are most likely, the difference is small and cancelled out by the overall increase in true positive rate.

Sensitivity to different magnitudes of outliers. To better understand outlier detection performance, we break down the results by magnitude of outliers in Figure 15. When outliers result from minor changes in demand levels, they are difficult to detect,

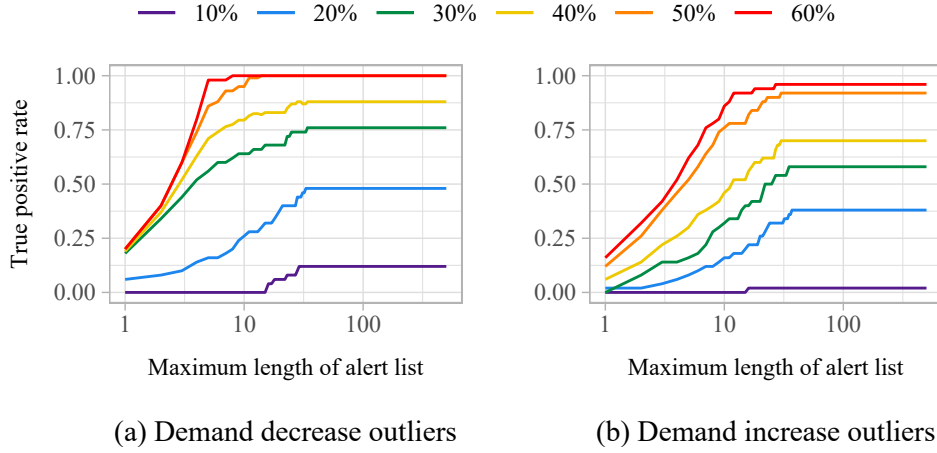


Figure 15: Sensitivity of true positive rate from FD+Agg under different magnitudes of homogeneous demand-volume outliers

resulting in low true positive rates. Given the significant overlap between the distribution of outlier demand with a 10% change in magnitude and that of regular demand, this is to be expected. Therefore, 10% demand changes effectively provide a lower bound on how big an outlier needs to be in order to be detected.

As the magnitude of the outliers increases, they become easier to detect and true positive rates are higher, with peak rates reached with shorter alert lists. Thus, genuine outliers are more likely to be ranked higher when they are caused by larger demand

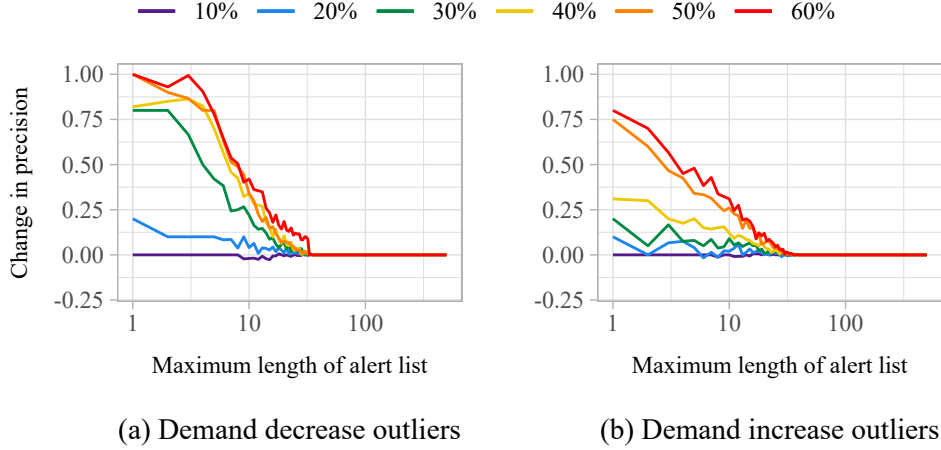


Figure 16: Sensitivity of precision from FD+Agg under different magnitudes of homogeneous demand-volume outliers

changes. For demand decreases of at least 50%, the true positive rate is very close to the optimal detection rate. Negative demand outliers are slightly easier to detect than positive demand outliers, meaning shorter alert lists are required. This is due to the demand censoring imposed by the booking controls and capacity restrictions.

Figure 16 shows the precision gap over randomly ordered lists. Once more, larger magnitude outliers result in larger precision improvements from ranking, while detecting minor outliers gains little over random selection. Similarly, we observe that detecting negative demand outliers gains slightly more precision in comparison to detecting positive outliers of the same magnitude. Additional results regarding false discovery rates are available in Appendix C.2.4.

5 Simulation Study: Forecast Adjustments for RM

To evaluate implications of adjusting the demand forecast for further planning steps, we simulate network demand and the optimisation of offered fare classes over the booking horizon. To this end, we first detail how the simulated RM system uses the demand forecast to compute revenue-optimal offers based on bid prices. In that, it follows a widely implemented industry standard. Subsequently, we describe alternative strategies that analysts may apply to adjust demand forecast based on identified outliers. Finally, by comparing revenue gained from offers based on different adjusted demand forecasts under the same simulated outlier demand, we highlight effects of adjustments as dependent on outlier scenarios.

5.1 Network revenue management system

The simulated RM system controls the offered set of fare classes per itinerary to optimise expected revenue. To that end, it implements a dynamic program to compute bid prices per leg and sums them up per itinerary – compare Strauss et al. (2018) and Appendix B.1 for technical details. The bid price indicates the marginal difference between the value of selling a seat in the current time period and that of reserving it to sell in a future time period. The RM system only offers fare classes where the revenue from a booking exceeds the bid price. Bid prices depend on time until departure, unsold capacity, and expected demand.

Booking patterns result as customers arrive and decide to book one of the offered fare classes. The firm does not report booking patterns for each individual itinerary, but only records them on the leg level.

Parameterising the dynamic program requires a forecast of expected demand arrival rates per leg l , fare class j , and time slice t of the booking horizon. Given that we know the underlying demand model for each itinerary in the simulation, we can estimate the arrival rates for each leg l and fare class j by:

$$\hat{\Lambda}_{j,l}(t) = \sum_{o \in \mathcal{O}_l} \sum_{i \in \mathcal{I}} p_{i,j,o} \lambda_{i,o}(t), \quad (12)$$

where $\lambda_{i,o}(t)$ is the arrival rate of customers of type i requesting itinerary o , and \mathcal{O}_l is the set of itineraries which include leg l . This creates an artificially accurate demand forecast. Deriving the demand forecast from the actual demand parameter values ensures that the estimation of revenue loss caused by undetected outliers is not affected by flawed forecasts (see Section 5.3). In practice, demand parameter values are not known but are estimated based on previously observed demand and time series forecasting.

5.2 Forecast adjustments for outlier demand

One aim of identifying outlier demand in booking patterns is to support analyst adjustments in RM systems. Without such adjustments, offers would be optimised for a regular demand forecast and thereby not be fit for maximising revenue under outlier demand. This raises the difficult issue of predicting the consequences from analyst adjustments throughout the network. As a step in this direction, we analyse a best-case-scenario, assuming that the adjustment is made with foresight, before the start of the booking horizon. We compare the revenue under three different adjustments:

- **Adjustment 1 (conservative):** Adjust only forecasts of affected single-leg itineraries. E.g., for an outlier creating additional demand for itinerary AC, increase the forecasts of itineraries AB and BC.
- **Adjustment 2 (aggressive):** Adjust forecasts of all itineraries that include at least one of the affected legs. E.g., for additional demand for itinerary AC, adjust all

itineraries including either leg AB or leg BC – i.e., itineraries AB, AC, AD, AE, BC, BD, and BE.

- **Adjustment 3 (balanced):** Adjust forecasts of affected single-leg itineraries and the *cluster-spanning* itinerary – in this case, AE. E.g., for additional demand for itinerary AC, adjust itineraries AB, BC, and AE. The motivation for adjusting AE (ahead of other itineraries) is that in general this will be the most popular itinerary in the cluster.

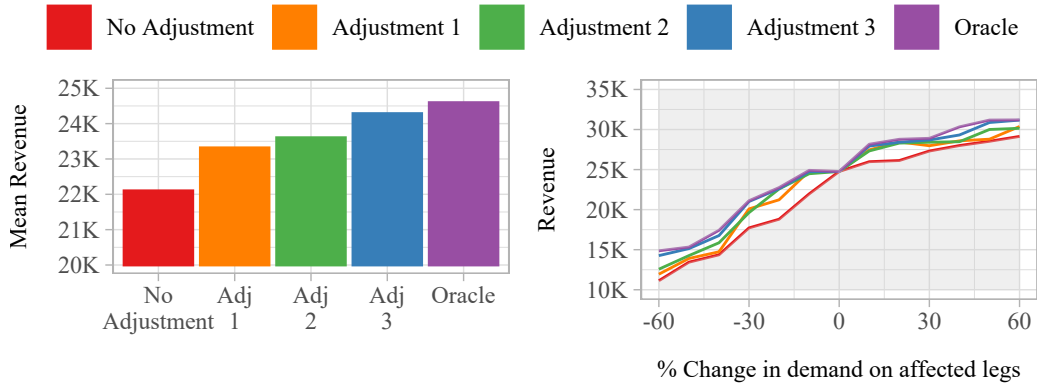
These three adjustments are not the only choices available to analysts. However, they represent options that stretch across the spectrum of how fully network effects are to be taken into account. Adjustments 1 (conservative, leg-based adjustments only) and 2 (aggressive, all potential network effects) are the two extremes. Adjustment 3 (balanced) is a compromise, which is more conservative than Adjustment 2 but still identifies the itinerary most likely to be the source of outlier demand. Further options would be to include more than just the cluster-spanning itinerary in an alternative to Adjustment 3, but this leaves another choice of which itineraries to prioritise. As a lower bound, we compute the revenue when **no adjustment** is made. As an upper bound, we implement an **oracle adjustment**, i.e., only adjusting the forecasts of affected itineraries. We compare the revenue as the level of outlier demand ranges from -60% to +60% of the average leg demand.

5.3 Experimental Results: Revenue Benefits

Figure 17 shows the revenue generated by outlier demand for each of the three adjustments. We show the results for four of ten itineraries contained within these four legs, compare Figure 11. The results for the other six itineraries are similar. Appendix C.3 details these results as well as further results on adjustments after outlier detection.

When outlier demand affects all four legs in the cluster (Figure 17a), any type of adjustment is always better than no adjustment. Besides the oracle, the best choice is Adjustment 3, i.e., the balanced approach, which adjusts the forecasts of the cluster-spanning itinerary and the individual leg. Adjustment 3 is able to obtain, on average, 87% of the additional revenue gained under the oracle adjustment. Similar results are obtained when the outlier demand affects three legs (Figure 17b).

When outlier demand affects only a single-leg itinerary (Figure 17d), the conservative Adjustment 1 and the oracle adjustment coincide. The aggressive Adjustment 2 yields less revenue than no adjustment. For example, although leg AB is correctly adjusted, the erroneous adjustment to itineraries AC, AD, and AE results in incorrect forecasts for legs BC, CD, and DE. The asymmetry between adjustment to positive and negative outlier demand is due to the level of demand being bounded below by 0. Similar results emerge when the outlier affects only two of the affected legs (Figure 17c), though the negative consequences of over-adjusting all potentially affected itineraries are less severe, as this



(a) Four leg itinerary (AE): mean revenue (left), revenue by demand change (right)

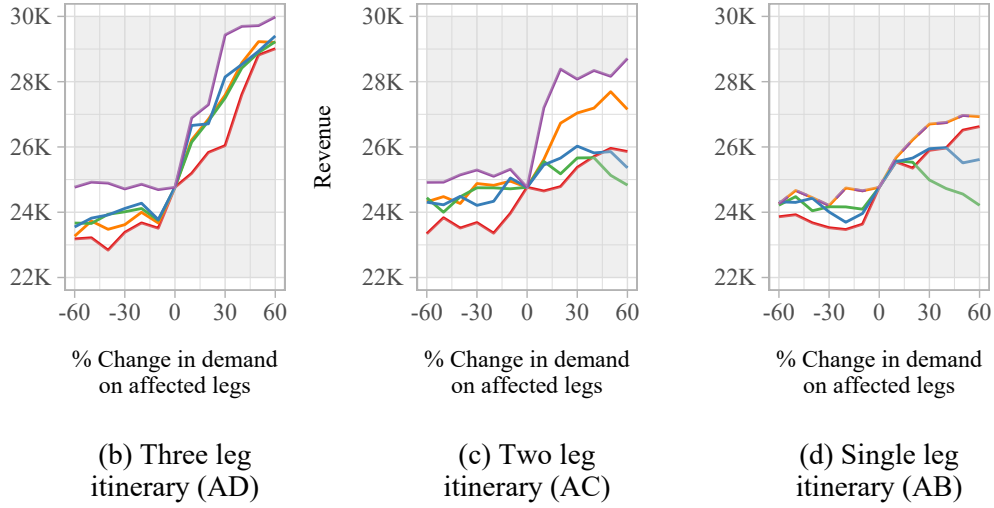


Figure 17: Revenue under different forecast adjustments; the subtitle indicates the actual outlier source

causes fewer superfluous adjustments.

The negative impact of adjusting unaffected itineraries highlights the importance of correctly clustering legs ahead of outlier detection. The closer the outlier demand itinerary is to the cluster spanning itinerary, the less risky it is to adjust all affected itineraries within a cluster, and the more benefit can be gained from doing so. From a managerial perspective, the *best* adjustment (other than the oracle) depends on the firm's objective. To maximise revenue when the most common outlier (e.g. itinerary AE) occurs, the balanced Adjustment 3 is preferable. Conversely, if the objective is to minimise risk to revenue even in the more unlikely scenarios (e.g. an outlier in itinerary AB), conservative Adjustment 1 is preferable. Overall, however, there are clear benefits from forecast adjustment.

6 Conclusion and outlook

In this paper, we proposed a two-step method for (i) clustering legs in a mobility network that are likely to benefit from joint outlier detection, and (ii) detecting outlying demand within such clusters. Furthermore, the proposed method, FD+AGG, ranks identified outliers according to their severity, creating an alert list to aid analysts in prioritising demand forecast adjustments.

The simulation study demonstrated the robustness of the method in a range of outlier demand scenarios. It highlighted that aggregating the analysis across clustered legs improves both detection rate and precision. Further, the ranked alert list correctly identified the most critical outliers. The advantages of the proposed approach became particularly clear when benchmarking its true positive rate, distribution of outliers across ranks, and precision, against that from a combination of Principal Component Analysis and High Density Regions (PCA+HDR) and on the non-ranked, leg-based method proposed in Rennie et al. (2021).

Furthermore, we implemented a simulated revenue management system to measure the potential revenue benefits of identifying and adjusting for demand outliers in a network setting by applying forecast adjustments. This analysis showed that taking into account the similarity of the legs can improve revenue in most scenarios. In the less likely scenario where only one or two legs of a cluster are affected by outlier demand, risk-averse firms may prefer leg-level adjustments.

Finally, by applying the proposed approach to empirical booking data collected by Deutsche Bahn, we demonstrated its applicability to the type of data observed in practice. In particular, we used this analysis to showcase the expected cluster results and to demonstrate how to account for additional practical considerations, such as trend and seasonality. Note that once the clustering has been performed, then the outlier detection can be performed in parallel within each cluster. Therefore our methodology is scalable to a much larger data set, such as the entire Deutsche Bahn long-distance train network. Such an analysis is not included in this paper as, beyond giving excessive insight into confidential company data, the research insight to be gained from visualising even more complex network cut-outs is limited.

Further research is needed to consider the practical aspects of outlier detection from the perspective of decision support. Notably, outlier detection can have broader benefits for operational planning in transportation networks, helping service providers to avoid overcrowding and delays. To realise such benefits, future research should particularly focus on effective ways to visualise outliers in networks and to communicate alert list to planners. An interesting avenue of further research would be to incorporate a feedback element whereby analysts mark outlier alerts as useful or not useful. A supervised learning approach, e.g. one-class-classifiers, could then be combined with our proposed outlier

detection routine to filter out false alerts.

Another research opportunity would be to consider how the aggregated outlier detection may be adapted for other areas of RM, e.g. in hotels, where correlation is induced by bookings for multiple consecutive nights. In particular, investigating the use of alternative clustering approaches is of interest - especially where the clusters are likely to be of different structures compared to the rail industry, e.g. in the airline industry where hub and spoke networks are more common than lines. Whilst this paper relied on clustering to improve outlier detection, we believe that the clustering approach is a useful contribution in and of itself. For example, clustering presents additional research avenues such as its application to improving network-level forecasting; supporting the planning for future new stations; evaluating how the transport network structure is changing over time; or defining different travel zones.

Acknowledgements

We gratefully acknowledge the support of the Engineering and Physical Sciences Research Council funded EP/L015692/1 STOR-i Centre for Doctoral Training. The authors acknowledge Deutsche Bahn for the provision of data, and are grateful to Philipp Bartke and Valentin Wagner for helpful discussions and suggestions.

References

- Amelio, A. and Pizzuti, C. (2015). Is normalized mutual information a fair measure for comparing community detection methods? *Proceedings of the 2015 IEEE/ACM International Conference on Advances in Social Networks Analysis and Mining, ASONAM 2015*, pages 1584–1585.
- Augustin, K., Gerike, R., Martinez Sanchez, M. J., and Ayala, C. (2014). Analysis of intercity bus markets on long distances in an established and a young market: The example of the U.S. and Germany. *Research in Transportation Economics*, 48:245–254.
- Barrow, D. and Kourentzes, N. (2018). The impact of special days in call arrivals forecasting: A neural network approach to modelling special days. *European Journal of Operational Research*, 264(3):967–977.
- Currie, C. S. M. and Rowley, I. T. (2010). Consumer behaviour and sales forecast accuracy: what’s going on and how should revenue managers respond? *Journal of Revenue and Pricing Management*, 9:374–376.
- De Baets, S. and Harvey, N. (2020). Using judgment to select and adjust forecasts from statistical models. *European Journal of Operational Research*, 284(3):882–895.

- Dubin, J. A. and Müller, H. G. (2005). Dynamical correlation for multivariate longitudinal data. *Journal of the American Statistical Association*, 100:872–881.
- Fawcett, L. and Walshaw, D. (2007). Improved estimation for temporally clustered extremes. *Environmetrics*, 18(2):173–188.
- Fawzy, A., Mokhtar, H. M., and Hegazy, O. (2013). Outliers detection and classification in wireless sensor networks. *Egyptian Informatics Journal*, 14(2):157–164.
- Febrero, M., Galeano, P., and González-Manteiga, W. (2008). Outlier detection in functional data by depth measures, with application to identify abnormal NOx levels. *Environmetrics*, 19(4):331–345.
- Grimshaw, S. D. (1993). Computing maximum likelihood estimates for the generalized pareto distribution. *Technometrics*, 35(2):185–191.
- He, G., Müller, H. G., and Wang, J. L. (2003). Functional canonical analysis for square integrable stochastic processes. *Journal of Multivariate Analysis*, 85(1):54–77.
- Hubert, M., Claeskens, G., De Ketelaere, B., and Vakili, K. (2012). A new depth-based approach for detecting outlying curves. In Colubi, A., Fokianos, K., Gonzalez-Rodriguez, G., and Kontogiorgos, E., editors, *Proceedings of COMPSTAT 2012*, pages 329–340.
- Hyndman, R. J. (1996). Computing and Graphing Highest Density Regions. *The American Statistician*, 50(2):120–126.
- Hyndman, R. J., Wang, E., and Laptev, N. (2016). Large-Scale Unusual Time Series Detection. *Proceedings - 15th IEEE International Conference on Data Mining Workshop, ICDMW 2015*, pages 1616–1619.
- Kendall, M. G. (1938). A new measure of rank correlation. *Biometrika*, 30:81–93.
- Klein, R., Koch, S., Steinhardt, C., and Strauss, A. K. (2020). A review of revenue management: Recent generalizations and advances in industry applications. *European Journal of Operational Research*, 284(2):397–412.
- Lawrence, M., Goodwin, P., O’Connor, M., and Onkal, D. (2006). Judgmental forecasting: A review of progress over the last 25 years. *International Journal of Forecasting*, 22(3):493–518.
- Leadbetter, M. (1991). On a basis for ‘Peaks over Threshold’ modeling. *Statistics and Probability Letters*, 12(4):357–362.
- Liang, T., Liu, H., and Tan, Y. (2020). Research on the gravity planning model of prefecture city rail transit network. *International Academic Exchange Conference on Science and Technology Innovation 2019*, 145(02005):493–518.

- Pearson, K. (1895). VII. Note on regression and inheritance in the case of two parents. *Proc. R. Soc. Lond.*, 58.
- Perera, H. N., Hurley, J., Fahimnia, B., and Reisi, M. (2019). The human factor in supply chain forecasting: A systematic review. *European Journal of Operational Research*, 274(2):574–600.
- Peter, S. J. and Victor, S. P. (2010). A novel algorithm for informative meta similarity clusters using minimum spanning tree. *International Journal of Computer Science and Information Security*, 8(1).
- Pickands, J. (1975). Statistical Inference using Extreme Order Statistics. *The Annals of Statistics*, 3(1):119–131.
- Prim, R. (1957). Shortest connection networks and some generalizations. *Bell Systems Technology Journal*, 36:1389–1401.
- Qu, H., Zhou, H., and Wu, Y. (2007). Controllable and Progressive Edge Clustering for Large Networks. *Graph Drawing. Lecture Notes in Computer Science*, 4372.
- Ramsay, J. O. and Silverman, B. W. (1997). *Functional Data Analysis*. Springer, New York.
- Ranshous, S., Shen, S., Koutra, D., Harenberg, S., Faloutsos, C., and Samatova, N. F. (2015). Anomaly detection in dynamic networks: A survey. *WIRES: Computational Statistics*, 7(3):223–247.
- Rennie, N., Cleophas, C., Sykulski, A. M., and Dost, F. (2021). Identifying and responding to outlier demand in revenue management. *European Journal of Operational Research*, 293:1015–1030.
- Ribatet, M. and Dutang, C. (2019). *POT: Generalized Pareto Distribution and Peaks Over Threshold*. R package version 1.1-7.
- Schaeffer, S. E. (2007). Graph clustering. *Computer Science Review*, 1(1):27–64.
- Schütze, C., Cleophas, C., and Tarafdar, M. (2020). Revenue management systems as symbiotic analytics systems: insights from a field study. *Business Research*, 13(3):1007–1031.
- Smith, R. L. (1985). Maximum Likelihood Estimation in a Class of Nonregular Cases. *Biometrika*, 72(1):67–90.
- Strauss, A. K., Klein, R., and Steinhardt, C. (2018). A review of choice-based revenue management: Theory and methods. *European Journal of Operational Research*, 271(2):375–387.

- Talagala, P. D., Hyndman, R. J., Smith-Miles, K., Kandanaarachchi, S., and Muñoz, M. A. (2019). Anomaly Detection in Streaming Nonstationary Temporal Data. *Journal of Computational and Graphical Statistics*.
- Talluri, K. T. and Van Ryzin, G. J. (2004). *The Theory and Practice of Revenue Management*. Kluwer Academic Publishers.
- Weatherford, L. R. (2016). The history of forecasting models in revenue management. *Journal of Revenue and Pricing Management*, 15(3):212–221.
- Weatherford, L. R. and Belobaba, P. P. (2002). Revenue impacts of fare input and demand forecast accuracy in airline yield management. *The Journal of the Operational Research Society*, 53(8):811–821.
- Weatherford, L. R. and Bodily, S. E. (1992). A taxonomy and research overview of perishable-asset revenue management: Yield management, overbooking, and pricing. *Operations Research*, 40:831–844.
- Weatherford, L. R. and Kimes, S. E. (2003). A comparison of forecasting methods for hotel revenue management. *International Journal of Forecasting*, 19(3):401–415.
- Yang, K. and Shahabi, C. (2004). A PCA-based similarity measure for multivariate time series. *MMDB 2004: Proceedings of the Second ACM International Workshop on Multimedia Databases*, pages 65–74.
- Yuan, W., Nie, L., Wu, X., and Fu, H. (2018). A dynamic bid price approach for the seat inventory control problem in railway networks with consideration of passenger transfer. *PloS one*, 13(8):e0201718.
- Zahn, C. T. (1971). Graph-Theoretical Methods for Detecting and Describing Gestalt Clusters. *IEEE Transactions on Computers*, C-20(1):68–86.

Appendices

A Additional details of method

Appendix A provides additional details on the proposed method described in Section 2, including the specifics of the correlation-based minimum spanning tree clustering, and the calculation of the functional depths.

A.1 Functional dynamical correlation

Let $y_{n,ij}(t)$ be the total observed bookings for the n^{th} departure on leg ij up to booking interval t , and similarly for $y_{n,jk}(t)$. The functional dynamical correlation between the booking patterns $y_{n,ij}(t)$ and $y_{n,jk}(t)$ is:

$$\rho_n(ij, jk) = \mathbb{E}\langle y_{n,ij}^*(t), y_{n,jk}^*(t) \rangle. \quad (13)$$

where

$$\langle y_{n,ij}^*(t), y_{n,jk}^*(t) \rangle = \int y_{n,ij}^*(t) y_{n,jk}^*(t) w(t) dt, \quad (14)$$

and $w(t)$ is a weight function that accounts for the time gap between observations. Here, $y_{n,ij}^*(t)$ is a standardised version of $y_{n,ij}(t)$:

$$y_{n,ij}^*(t) = \frac{y_{n,ij}(t) - M_{ij} - \mu_{ij}(t)}{\left[\int \{y_{n,ij}(t) - M_{ij} - \mu_{ij}(t)\}^2 w(t) dt \right]^{1/2}}, \quad (15)$$

where $\mu_{ij}(t)$ is a mean function, and:

$$M_{ij} = \langle y_{n,ij}(t), 1 \rangle. \quad (16)$$

The functional dynamical correlation is then the average across all N departures:

$$\rho(ij, jk) = \frac{1}{N} \sum_{n=1}^N \rho_n(ij, jk). \quad (17)$$

A.2 Prim's algorithm

Prim's algorithm is a greedy algorithm with the following basic steps. Assuming the original graph G has $V(G)$ vertices.

- Initialise the MST, T , with the edge with minimum weight and the two vertices it connects. Let $V(T)$ be the number of edges in T .
- While $V(T) < V(G)$:
 - go through the remaining edges in G in order from smallest to largest weights, until one is found that is connected to T , but does not form a circuit (i.e. the edge does not form a loop such that T is no longer a tree).

- Add this edge (and the vertices it connects) to T .

More computationally efficient algorithms exist but given the reasonable size of the graphs considered, and more specifically their sparsity (very few stations are adjacent), computational time is reasonable using Prim's algorithm.

A.3 Functional depth

The functional halfspace depth is given by:

$$d_{nl}(\mathbf{y}_{nl} \in \mathcal{Y}_l; \alpha) = \sum_{j=1}^T w_\alpha(t_j) HD_j(\mathbf{y}_{nl}(t_j)), \quad (18)$$

where, using $t_{\tau+1} = t_\tau + 0.5(t_\tau - t_{\tau-1})$, the weights $w_\alpha(t_j)$ are, according to Hubert et al. (2012):

$$w_\alpha(t_j) = \frac{(t_{j+1} - t_j) \text{vol} [\{\mathbf{x} \in \mathbb{R}^k : HD_j(\mathbf{x}) \geq \alpha\}]}{\sum_{j=1}^T (t_{j+1} - t_j) \text{vol} [\{\mathbf{x} \in \mathbb{R}^k : HD_j(\mathbf{x}) \geq \alpha\}]}, \quad (19)$$

where $\alpha \in (0, 0.5]$, with a default value of $\alpha = 1/T$. The sample halfspace depth of a K -variate vector x at time t_j is given by (Hubert et al., 2012):

$$HD_j(y_{nl}(t_j)) = \frac{1}{N} \min_{\mathbf{u}, \|\mathbf{u}\|=1} \# \{y_{nl}(t_j), n = 1, \dots, N : \mathbf{u}^T y_{nl}(t_j) \geq \mathbf{u}^T \mathbf{x}\} \quad (20)$$

A.4 Normalised Mutual Information

For a graph containing M legs, the mutual information between two clusterings \mathcal{A} and \mathcal{B} of the M nodes in the inverted graph is defined as:

$$I(\mathcal{A}, \mathcal{B}) = \sum_{a=1}^{|\mathcal{A}|} \sum_{b=1}^{|\mathcal{B}|} \frac{|\mathcal{A} \cap \mathcal{B}|}{M} \log \left(|\mathcal{A} \cap \mathcal{B}| \frac{M}{M_a M_b} \right), \quad (21)$$

where M_a is the number of nodes in the a^{th} cluster of clustering \mathcal{A} , and similarly for M_b . The **normalised mutual information (NMI)** between two clusterings is defined as (Amelio and Pizzuti, 2015):

$$NMI(\mathcal{A}, \mathcal{B}) = \frac{2I(\mathcal{A}, \mathcal{B})}{H(\mathcal{A}) + H(\mathcal{B})}, \quad (22)$$

where $H(\mathcal{A})$ is the entropy (a measure of uncertainty) defined as:

$$H(\mathcal{A}) = - \sum_{a=1}^{|\mathcal{A}|} \frac{M_a}{M} \log \left(\frac{M_a}{M} \right). \quad (23)$$

$NMI(\mathcal{A}, \mathcal{B}) = 1$ if \mathcal{A} and \mathcal{B} are identical, and 0 if they are completely different.

B Details of computational study

Appendix B contains additional details of the simulation set up described in Section 4, including the computation of the bid prices, and a validation of the chosen parameter values.

B.1 Dynamic programming for bid price control

From Talluri and Van Ryzin (2004), let x be the remaining capacity, and define $V_t(x)$ denote the value function at time t . Define $R(t)$:

$$R(t) = \begin{cases} r_j & \text{if request for fare class } j \text{ arrives in interval } t \\ 0 & \text{otherwise} \end{cases} \quad (24)$$

where r_j denotes the revenue from accepting a request for fare class j . The probability that $R(t) = r_j$ is equal to the arrival rate for fare class j at time t . Note the arrival rates are such that at most one request arrives in each time period. Define:

$$u = \begin{cases} 1 & \text{if request for fare class } j \text{ arrives **and** is accepted} \\ 0 & \text{otherwise} \end{cases} \quad (25)$$

We wish to maximise the combined revenue in the current time period, and the revenue to come in future time periods:

$$\max_{u \in \{0,1\}} (R(t)u + V_{t+1}(x - u)) \quad (26)$$

The Bellman equation for $V_t(x)$ is:

$$V_t(x) = \mathbb{E} \left[\max_{u \in \{0,1\}} \{R(t)u + V_{t+1}(x - u)\} \right] \quad (27)$$

$$= V_{t+1}(x) + \mathbb{E} \left[\max_{u \in \{0,1\}} \{(R(t) + \Delta V_{t+1}(x))u\} \right] \quad (28)$$

$$V_t(x) = \sum_{j=1}^{|\mathcal{J}|} \lambda_j(t) \max \{ (r_j - \Delta V_{t+1}(x)), 0 \} \quad (29)$$

where $\lambda_j(t)$ is the arrival rate of demand for fare class j in interval t , and $\Delta V_{t+1}(x) = V_{t+1}(x) - V_{t+1}(x-1)$ is the marginal cost of capacity in the next time period. The problem is solved with backwards recursion, with the following boundary conditions apply:

$$V_{T+1}(x) = 0, \quad x = 0, 1, \dots, C \quad (30)$$

$$V_t(0) = 0, \quad t = 1, \dots, T \quad (31)$$

These ensure (i) no revenue can be generated beyond the booking horizon i.e after departure; and (ii) that no further revenue can be generated if there is no capacity remaining. The bid price at time t with remaining capacity x is given by $\Delta V_t(x)$.

B.2 Details of benchmark method

We use the method proposed by Hyndman et al. (2016) as a benchmark comparison for our proposed method in Section 4. The method works as follows:

- Define the total demand booking patterns as the sum of the demand for each leg within the cluster.
- Compute f features of the n total demand booking patterns. Features include: mean, variance, first order autocorrelation, trend, linearity, seasonality, peak, trough, entropy, lumpiness, spikiness, change in variance, Kullback-Leibler score, among others. See Hyndman et al. (2016) for a full list.
- Apply principal component analysis (PCA) as per Yang and Shahabi (2004) to determine the first two principle components i.e. those that explain the most variance.
- Use a density-based multi-dimensional approach (Hyndman, 1996) to find points in the first two principal components with lowest density.
- The nu points with the lowest densities relate to the departures which are classified as outliers.

B.3 Parameter values for simulation study

Table 2: Regular demand generation parameter values

| Parameter | Value | Effect of parameter |
|---|--|---|
| $\alpha = \{\alpha_{AB}, \alpha_{AC}, \alpha_{AD}, \alpha_{AE}, \alpha_{BC}, \alpha_{BD}, \alpha_{BE}, \alpha_{CD}, \alpha_{CE}, \alpha_{DE}\}$ | $\alpha = \{32, 14, 14, 180, 4, 4, 14, 4, 14, 32\}$ | Parameters of the Gamma distribution which controls the level of total demand across all fare classes and customer types such that the mean demand for itinerary o is: $\mathbb{E}(D_o) = \frac{\alpha_o}{\beta_o}.$ |
| $\beta = \{\beta_{AB}, \beta_{AC}, \beta_{AD}, \beta_{AE}, \beta_{BC}, \beta_{BD}, \beta_{BE}, \beta_{CD}, \beta_{CE}, \beta_{DE}\}$ | $\beta = \{1, 1, 1, 1, 1, 1, 1, 1, 1, 1\}$ | |
| $\mathbf{a_1} = \{a_{1,AB}, a_{1,AC}, a_{1,AD}, a_{1,AE}, a_{1,BC}, a_{1,BD}, a_{1,BE}, a_{1,CD}, a_{1,CE}, a_{1,DE}\}$ | $\mathbf{a_1} = \{5, 5, 5, 5, 5, 5, 5, 5, 5, 5\}$ | Parameters of Beta distribution which controls the arrival times of type 1 customers |
| $\mathbf{b_1} = \{b_{1,AB}, b_{1,AC}, b_{1,AD}, b_{1,AE}, b_{1,BC}, b_{1,BD}, b_{1,BE}, b_{1,CD}, b_{1,CE}, b_{1,DE}\}$ | $\mathbf{b_1} = \{2, 2, 2, 2, 2, 2, 2, 2, 2, 2\}$ | |
| $\mathbf{a_2} = \{a_{2,AB}, a_{2,AC}, a_{2,AD}, a_{2,AE}, a_{2,BC}, a_{2,BD}, a_{2,BE}, a_{2,CD}, a_{2,CE}, a_{2,DE}\}$ | $\mathbf{a_2} = \{2, 2, 2, 2, 2, 2, 2, 2, 2, 2\}$ | Parameters of Beta distribution which controls the arrival times of type 2 customers |
| $\mathbf{b_2} = \{b_{2,AB}, b_{2,AC}, b_{2,AD}, b_{2,AE}, b_{2,BC}, b_{2,BD}, b_{2,BE}, b_{2,CD}, b_{2,CE}, b_{2,DE}\}$ | $\mathbf{b_2} = \{2, 3, 5, 7, 2, 3, 5, 2, 3, 2\}$ | |
| $\mathbf{p_{1jo}} = \{p_{1Ao}, p_{1Oo}, p_{1Jo}, p_{1Po}, p_{1Ro}, p_{1So}, p_{1Mo}\}$ | $\mathbf{p_{1jo}} = \{0.30, 0.25, 0.20, 0.15, 0.10, 0, 0\}$ | Probability of purchase for each customer type. It is assumed these are constant across itineraries. The no-purchase probability for customer type i is equal to $1 - \sum_{j \in \mathcal{J}} p_{ijo}$. |
| $\mathbf{p_{2jo}} = \{p_{2Ao}, p_{2Oo}, p_{2Jo}, p_{2Po}, p_{2Ro}, p_{2So}, p_{2Mo}\}$ | $\mathbf{p_{2jo}} = \{0, 0.05, 0.10, 0.15, 0.20, 0.25, 0.25\}$ | |
| $\phi_o = \{\phi_{1,o}, \phi_{2,o}\}$ | $\phi_o = \{0.5, 0.5\} \forall o$ | Proportion of total demand from each customer type for each itinerary. It is assumed these are constant across itineraries. |

B.3.1 Outliers considered in computational study

Table 3 shows the different experiments that were carried out as part of the computational study. We consider *cluster* outliers in which every itinerary within the cluster is equally affected; *itinerary* outliers where only a single itinerary within the cluster is affected; and *station* outliers which affect all itineraries that end at a particular station.

| Experiment | Outlier Type | Itineraries Affected | Magnitudes |
|------------|--------------|----------------------|--|
| 1 | Cluster | All | +10%, +20%, +30%, +40%, +50%, +60%, -10%, -20%, -30%, -40%, -50%, -60% |
| 2 | Itinerary | AB | +50% |
| 3 | | AC | +50% |
| 4 | | AD | +50% |
| 5 | | AE | +50% |
| 6 | | BC | +50% |
| 7 | | BD | +50% |
| 8 | | BE | +50% |
| 9 | | CD | +50% |
| 10 | | CE | +50% |
| 11 | | DE | +50% |
| 12 | Station | AB | +50% |
| 13 | | AC, BC | +50% |
| 14 | | AD, BD, CD | +50% |
| 15 | | AE, BE, CE, DE | +50% |

Table 3: Different types of outliers considered in computational study

C Computational results

Appendix C includes the extended results from the computational study described in Section 4. Results from additional simulation experiments to test the proposed clustering approach are also presented here.

C.1 Evaluation of network clustering

For the correlation-based clustering to perform well it needs to (i) accurately estimate similarity between adjacent legs, and (ii) use information about pairwise similarity between adjacent legs to detect similarity between (potentially) more than two legs to form clusters. We use the proportion of total demand belonging to each itinerary to determine a clustering benchmark. For example, in Figure 18a, when *all* passengers travel the itinerary from A to E, the resulting bookings in each of the four legs would be identical. In this case, the correlation between legs would be 1 – giving a single cluster of four legs.

To evaluate the clustering when the underlying demand is known, we define the **common traffic ratio** between two adjacent legs as the proportion of total demand that relates to itineraries over both legs. That is, for two legs ij and jk , we define the common traffic ratio, $r(ij, jk)$, to be:

$$r(ij, jk) = \frac{D_{ik}}{D_{ij} + D_{jk} + D_{ik}}, \quad (32)$$

where D_{ij} is the demand for itinerary ij , and D_{ik} is the total demand for all itineraries which include both legs ij and jk . If all passengers book itineraries that traverse both legs, then $r(ij, jk) = 1$. Conversely, if no passengers book journeys that traverse both legs, then $r(ij, jk) = 0$.

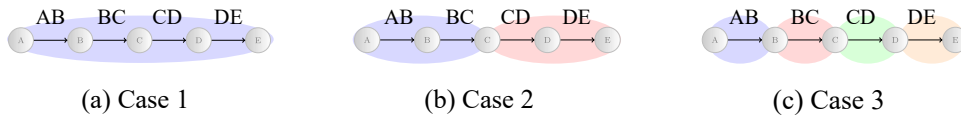


Figure 18: Benchmark clustering

We vary the level of demand for each itinerary to generate different benchmark clusterings. The output of the correlation-based clustering is then compared with benchmark clustering using the NMI. We consider three cases: the four legs belong in a single cluster (Figure 18a); they belong in two clusters (Figure 18b); and they belong in four clusters (Figure 18c).

- **Case 1:** When itinerary AE accounts for at least 50% of the network demand, we expect legs AB, BC, CD, and DE to belong to the same cluster, as they experience mostly

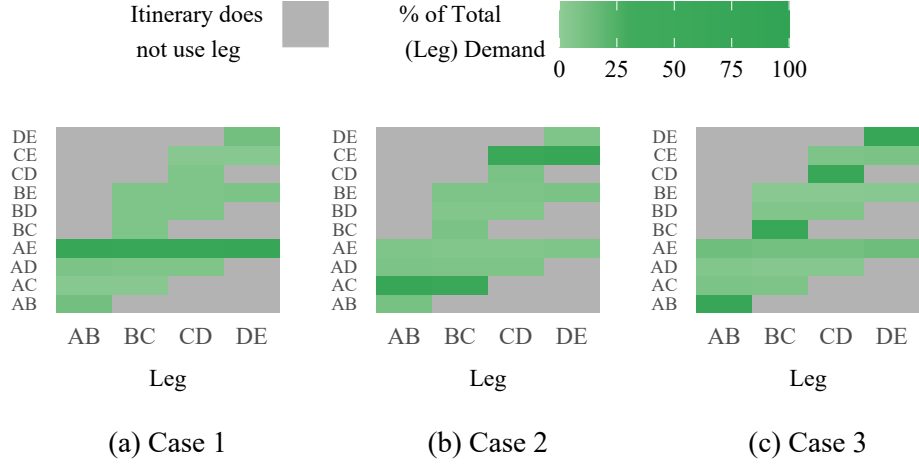


Figure 19: Itinerary demand per leg

the same demand. Remaining demand is calibrated across itineraries such that total demand for each leg is reasonably uniformly distributed. We compare the correlation-based clustering with the benchmark clustering of all four legs in a single cluster, when the average percentage of demand on each leg from itinerary AE is 50%, 60%, 70%, 80%, 90%, or 100%. Figure 19a shows the fraction of total demand on each leg, from each itinerary, in the case where 60% of demand is for itinerary AE.

- **Case 2:** We calibrate the majority of demand on leg AB and BC to be for itinerary AC, and the majority of demand on legs CD and DE to be demand for itinerary CE. For simplicity, the distribution of demand is symmetric across the four legs. We compare the performance when the average percentage of demand on each leg belonging to the clustering benchmark itinerary is 50%, 60%, 70%, 80%, 90%, or 100%. Figure 19b shows the case where 60% of demand on each leg is for the respective cluster itineraries (AC or CE).
- **Case 3:** We calibrate the majority of demand on leg AB for itinerary AB, the majority of demand on leg BC for itinerary BC, and so on. We compare the performance when the average percentage of demand on each leg belonging to the leg itinerary is 50%, 60%, 70%, 80%, 90%, or 100%. Figure 19c shows the case where 60% of demand on each leg is for the itinerary consisting of only that leg.

The results are shown in Table 4.

In almost all cases, the normalised mutual information between the correlation-based clustering and the benchmark equals 1, indicating congruence. We now extend the simulation study by comparing the output of the correlation-based clustering under different correlation measures. In addition to the functional dynamical correlation measure described in Section 2.1, we compare *Pearson correlation* (Pearson, 1895) and *Kendall rank*

| | Fraction of Leg Demand Resulting from Cluster Itinerary Demand | | | | | |
|---------------|--|------|------|------|------|------|
| | 50% | 60% | 70% | 80% | 90% | 100% |
| Case 1 | 0.99 | 1.00 | 1.00 | 1.00 | 1.00 | 1.00 |
| Case 2 | 0.98 | 0.99 | 1.00 | 1.00 | 1.00 | 1.00 |
| Case 3 | 0.94 | 0.97 | 0.99 | 1.00 | 1.00 | 1.00 |

Table 4: Normalised mutual information

correlation (Kendall, 1938). Let $y_{n,ij}(t)$ be the observed bookings for the n^{th} departure on leg ij , and $y_{n,pq}(t)$ analogous for leg pq .

- **Pearson correlation:** calculate the Pearson correlation between corresponding booking patterns, then average across all booking patterns. That is, for the n^{th} of N booking patterns observed over T booking intervals, we calculate the Pearson correlation coefficient as:

$$\rho_n(ij, pq) = \frac{\sum_{t=1}^T (y_{n,ij}(t) - \overline{y_{n,ij}})(y_{n,pq}(t) - \overline{y_{n,pq}})}{\sqrt{\sum_{t=1}^T (y_{n,ij}(t) - \overline{y_{n,ij}})^2} \sqrt{\sum_{t=1}^T (y_{n,pq}(t) - \overline{y_{n,pq}})^2}} \quad (33)$$

where $\overline{y_{n,ij}}$ is the mean number of bookings for the n^{th} booking pattern. Then:

$$\rho(ij, pq) = \frac{1}{n} \sum_{n=1}^N \rho_n(ij, pq). \quad (34)$$

- **Kendall rank correlation:** observations $(y_{n,ij}(s), y_{n,pq}(s))$ and $(y_{n,ij}(t), y_{n,pq}(t))$ where $s < t$, are *concordant* if their ordering agrees, and *discordant* otherwise. The Kendall rank correlation is defined between the n^{th} booking patterns in legs ij and pq as:

$$\rho_n(ij, pq) = \frac{t_c - t_d}{\sqrt{(t_0 - t_1)(t_0 - t_2)}} \quad (35)$$

where t_c is the number of concordant pairs, t_d is the number of discordant pairs, and t_0 , t_1 , and t_2 are defined as follows:

$$t_0 = \frac{T(T-1)}{2}, \quad (36)$$

$$t_1 = \sum_s u_s(u_s - 1)/2, \quad (37)$$

$$t_2 = \sum_t v_t(v_t - 1)/2, \quad (38)$$

where u_s is the number of tied values in the s^{th} group of ties for in booking patterns for leg ij , and v_t is analogous for leg pq . Then:

$$\rho(ij, pq) = \frac{1}{n} \sum_{n=1}^N \rho_n(ij, pq). \quad (39)$$

We compare the cases where the correlation measure is (i) applied directly to the booking patterns, and (ii) applied to the differenced booking patterns where the within-booking pattern relationships e.g. trend have been removed. The normalised mutual information between the clustering produced by the correlation-based clustering under each of the different correlation measures, and the benchmark clustering is shown in Table 5.

| Case | Correlation Measure | Fraction of Leg Demand Resulting from Cluster Itinerary Demand | | | | | |
|--------|----------------------------------|---|------|------|------|------|------|
| | | 50% | 60% | 70% | 80% | 90% | 100% |
| Case 1 | Booking patterns | | | | | | |
| | Functional dynamical correlation | 0.99 | 1.00 | 1.00 | 1.00 | 1.00 | 1.00 |
| | Pearson correlation | 1.00 | 1.00 | 1.00 | 1.00 | 1.00 | 1.00 |
| | Kendall rank correlation | 1.00 | 1.00 | 1.00 | 1.00 | 1.00 | 1.00 |
| | Differenced booking patterns | | | | | | |
| | Functional dynamical correlation | 0.99 | 1.00 | 1.00 | 1.00 | 1.00 | 1.00 |
| | Pearson correlation | 0.98 | 1.00 | 1.00 | 1.00 | 1.00 | 1.00 |
| | Kendall rank correlation | 1.00 | 1.00 | 1.00 | 1.00 | 1.00 | 1.00 |
| Case 2 | Booking patterns | | | | | | |
| | Functional dynamical correlation | 0.98 | 0.99 | 1.00 | 1.00 | 1.00 | 1.00 |
| | Pearson correlation | 0.00 | 0.00 | 0.00 | 0.00 | 0.00 | 0.00 |
| | Kendall rank correlation | 0.00 | 0.00 | 0.00 | 0.00 | 0.00 | 0.00 |
| | Differenced booking patterns | | | | | | |
| | Functional dynamical correlation | 0.98 | 0.99 | 1.00 | 1.00 | 1.00 | 1.00 |
| | Pearson correlation | 0.00 | 0.00 | 0.00 | 0.00 | 0.00 | 0.00 |
| | Kendall rank correlation | 0.00 | 0.00 | 0.00 | 0.00 | 0.00 | 0.00 |
| Case 3 | Booking patterns | | | | | | |
| | Functional dynamical correlation | 0.94 | 0.97 | 0.99 | 1.00 | 1.00 | 1.00 |
| | Pearson correlation | 0.00 | 0.00 | 0.00 | 0.00 | 0.00 | 0.00 |
| | Kendall rank correlation | 0.00 | 0.00 | 0.00 | 0.00 | 0.00 | 0.00 |
| | Differenced booking patterns | | | | | | |
| | Functional dynamical correlation | 0.93 | 0.96 | 0.99 | 1.00 | 1.00 | 1.00 |
| | Pearson correlation | 0.00 | 0.00 | 0.00 | 0.00 | 0.00 | 0.00 |
| | Kendall rank correlation | 0.00 | 0.00 | 0.00 | 0.00 | 0.00 | 0.00 |

Table 5: Normalised mutual information under different correlation measures

For case 1, all three correlation measure seem to be performing equally well, with the normalised mutual information almost always indicating congruence. For cases 2 and 3, the Pearson and Kendall correlation results in extremely poor performance in terms of NMI, with the benchmark clustering never being achieved. Functional dynamical correlation, however, continues to perform well with an NMI close to 1.

In order to determine why the Pearson and Kendall rank correlations initially appear

to perform well in the single cluster case, but fail in the two cluster case, we also compare the value of the correlation coefficient with the known demand share in a simple two leg example. Consider the simple two leg network shown in Figure 20.

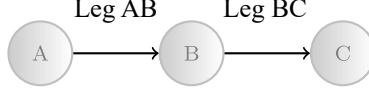


Figure 20: Network with two legs

The common traffic ratio of legs AB and BC is:

$$r(AB, BC) = \frac{D_{AC}}{D_{AB} + D_{BC} + D_{AC}}, \quad (40)$$

If $r(AB, BC) = 1$, then the number of bookings on leg AB and leg BC are identical, and the correlation between them is 1. Conversely, if $r(AB, BC) = 0$, then the bookings on leg AB and leg BC are independent with correlation 0. Table 6 shows the estimates of the correlation, compared to the true ratio, $r(AB, BC)$.

| $r(AB, BC)$ | 0.0 | 0.1 | 0.2 | 0.3 | 0.4 | 0.5 | 0.6 | 0.7 | 0.8 | 0.9 | 1.0 |
|--|------|------|------|------|------|------|------|------|------|------|------|
| Correlation between booking patterns | | | | | | | | | | | |
| Functional dynamical correlation | 0.12 | 0.22 | 0.35 | 0.40 | 0.46 | 0.55 | 0.66 | 0.82 | 0.86 | 0.90 | 1.00 |
| Pearson correlation | 0.99 | 0.99 | 0.99 | 1.00 | 1.00 | 1.00 | 1.00 | 1.00 | 1.00 | 1.00 | 1.00 |
| Kendall rank correlation | 0.99 | 0.99 | 0.99 | 0.99 | 0.99 | 0.99 | 0.99 | 0.99 | 1.00 | 1.00 | 1.00 |
| Correlation between differenced booking patterns | | | | | | | | | | | |
| Functional dynamical correlation | 0.14 | 0.18 | 0.29 | 0.42 | 0.50 | 0.53 | 0.66 | 0.83 | 0.88 | 0.91 | 1.00 |
| Pearson correlation | 0.70 | 0.71 | 0.77 | 0.82 | 0.85 | 0.89 | 0.92 | 0.95 | 0.96 | 0.98 | 1.00 |
| Kendall rank correlation | 0.88 | 0.90 | 0.91 | 0.91 | 0.92 | 0.94 | 0.94 | 0.95 | 0.96 | 0.97 | 1.00 |

Table 6: Comparison of correlation measures

Functional dynamical correlation, applied directly to the data, performs best in all cases. In case 1, where the benchmark clustering is a single cluster, poor clustering performance can only result from under-estimating the demand share. Both Pearson and Kendall rank correlation over-estimate the correlation between booking patterns, even when the within-booking pattern effects have been removed. This explains the good performance of Pearson and Kendall rank correlation in case 1, despite extremely poor performance in cases 2 and 3.

C.2 Detecting outliers in multiple legs

C.2.1 Experimental results on detecting outliers in multiple legs

Table 7 provides the results shown in Figure 12 in tabular format.

| Length of alert list | 1 | 5 | 10 | 50 | 100 | 250 | 500 |
|---------------------------|------|------|------|------|------|------|------|
| FD + Agg | 0.16 | 0.44 | 0.50 | 0.68 | 0.68 | 0.68 | 0.68 |
| PCA + HDR ($\nu = 5$) | 0.09 | 0.18 | 0.18 | 0.18 | 0.18 | 0.18 | 0.18 |
| PCA + HDR ($\nu = 10$) | 0.09 | 0.18 | 0.23 | 0.23 | 0.23 | 0.23 | 0.23 |
| PCA + HDR ($\nu = 50$) | 0.09 | 0.18 | 0.23 | 0.35 | 0.35 | 0.35 | 0.35 |
| PCA + HDR ($\nu = 100$) | 0.09 | 0.18 | 0.23 | 0.35 | 0.43 | 0.43 | 0.43 |
| PCA + HDR ($\nu = 250$) | 0.09 | 0.18 | 0.23 | 0.35 | 0.43 | 0.66 | 0.66 |
| PCA + HDR ($\nu = 500$) | 0.09 | 0.18 | 0.23 | 0.35 | 0.43 | 0.66 | 1 |

Table 7: True positive rate of FD+Agg in comparison to PCA+HDR benchmark under varying lengths of alert list

C.2.2 Outlier detection under different functional depth thresholds

We recognise that the percentage of departures that analysts are able to adjust strongly depends on the ratio of analysts to departures, and that this is likely to be domain dependent. Therefore, here we consider outlier detection performance as the functional depth threshold varies.

In terms of true positive rates, the choice of threshold of 0.01, 0.05, or 0.1 produces similar results, at least near the top of the alert list. Our method ranks the departures classified as outliers such that genuine outliers are more likely to be at the top of the ranked list, and false positives at the bottom of the list. Therefore, using a higher threshold tends to add more departures to the bottom of the list, and increase the risk of more false positives. As shown in Section 4 of the manuscript, the outliers that a threshold of 0.01 fails to detect tend to be small changes in magnitude. It is these small magnitude outliers that are added to the bottom of the list as the threshold increases. Notably, a threshold of 0.001 results in reduced performance even at the top of the list, suggesting this would be too low a threshold. Similar results are seen in the change in precision (compared to the non ranked method with the same threshold).

A higher threshold does result in higher overall true positive rates as more departures are classified as outliers. However, the maximum true positive rate for a threshold of 0.05 results in around 1 in 5 departures being classified as outliers. This is quite a high percentage for them all to be considered *outliers*.

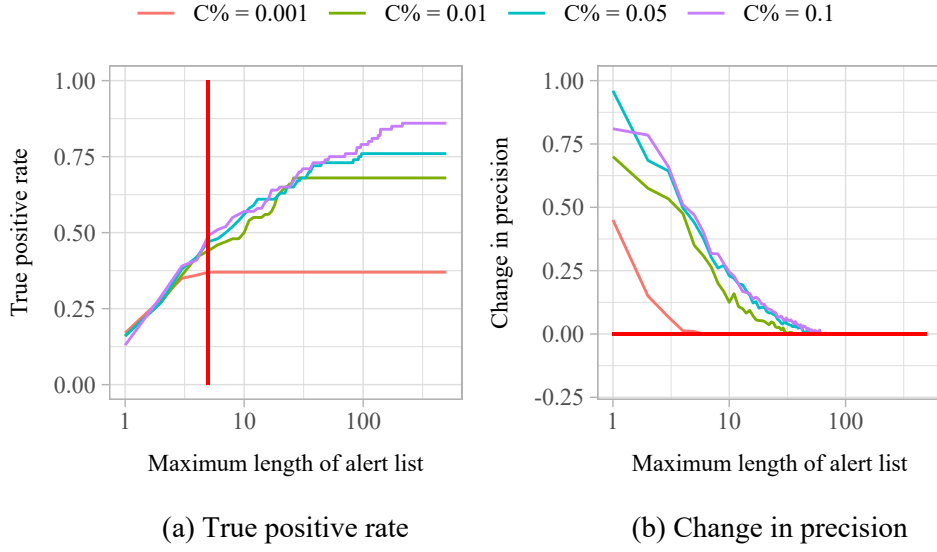


Figure 21: Outlier detection performance under different functional depth thresholds

C.2.3 Distribution of outliers across multiple legs

In the scenario where all itineraries are equally affected, a high proportion of outliers should be detected in more than one leg. Figure 22a illustrates the proportion of outliers detected in 1, 2, 3 or 4 legs: More than half were detected in multiple legs. Figure 22b shows the proportion of true positives (genuine outliers which were detected), by the number of legs in which they were detected. In contrast with Figure 22a, a much higher percentage of genuine outliers are detected in all four legs.

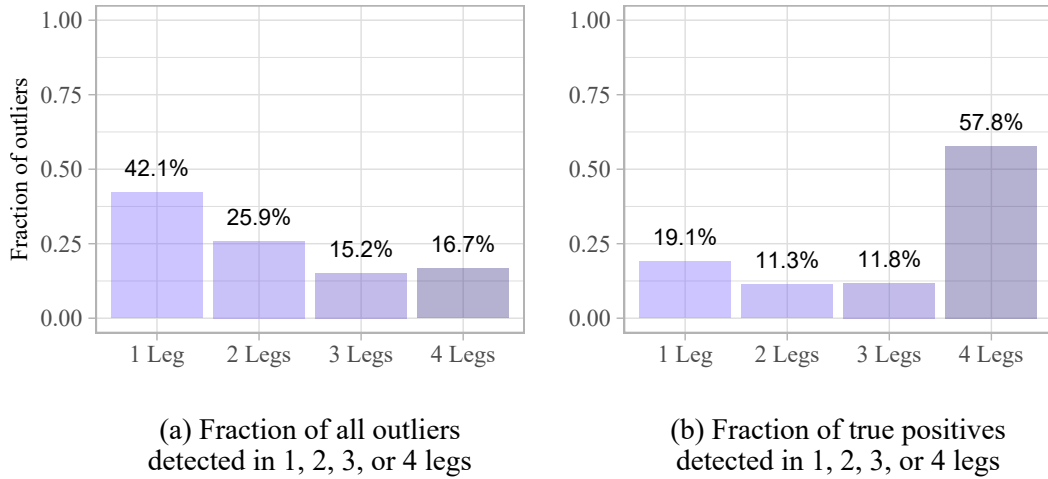


Figure 22: Fraction of outliers detected in 1, 2, 3, or 4 legs

Given the clustering is correct, we expect an approximately equal number of single leg outliers in each leg, as shown in Figure 23b. If one leg, say DE, had not belonged in this cluster, we would expect a higher proportion of single leg outliers to have been detected

in leg DE. This could be utilised as a method for checking the clustering, after the outlier detection.

These results motivate aggregating threshold exceedances across legs in two ways: (i) since less than 100% of genuine outliers were detected in all legs, if outlier detection was carried out only on the leg level, outliers could be missed on some legs. (ii) Given that a much higher proportion of outliers detected in four legs were genuine outliers, by ranking booking patterns detected in all legs as more likely to be outliers, we focus analysts' attention to those more likely to be genuine outliers.

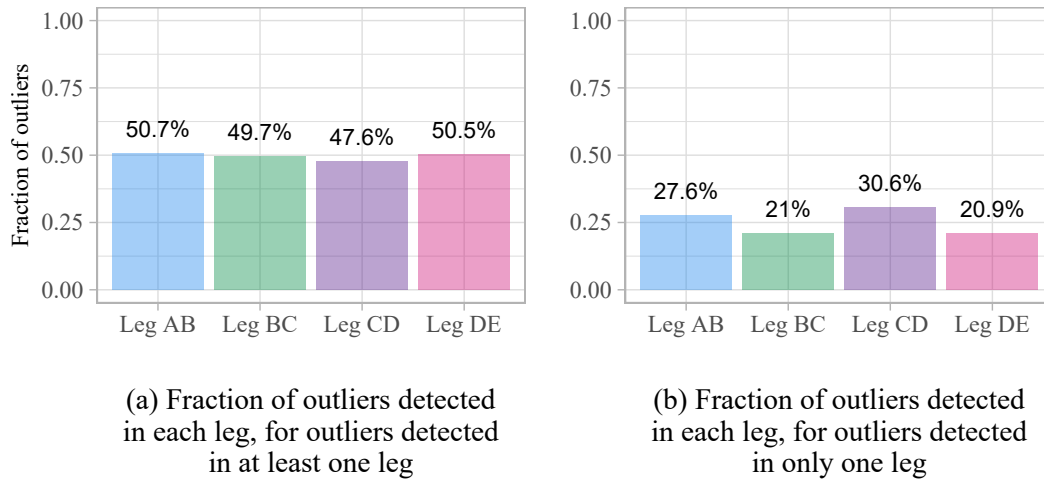


Figure 23: Fraction of outliers detected in each leg

C.2.4 False Discovery Rate

The *false discovery rate* (FDR) is defined as the proportion of booking patterns classified as outliers which were false positives:

$$FDR = \frac{FP}{TP + FP} \quad (41)$$

See Section 4.4 for definitions of true and false positives. Figure 24 shows the FDR for the case where outlier demand affects all itineraries, and the magnitude is randomly chosen from each of the distributions described in Section 4.2.

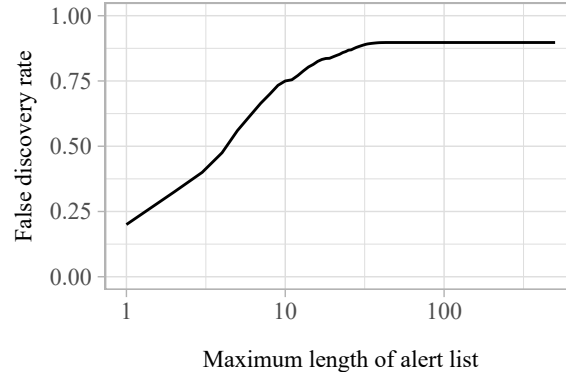


Figure 24: False discovery rate for nonhomogeneous demand-volume outliers

Figure 25 shows the FDR for each of the magnitudes of outliers considered in the simulation study. Given that smaller magnitude outliers are more similar to the regular demand, these result in higher false discovery rates.

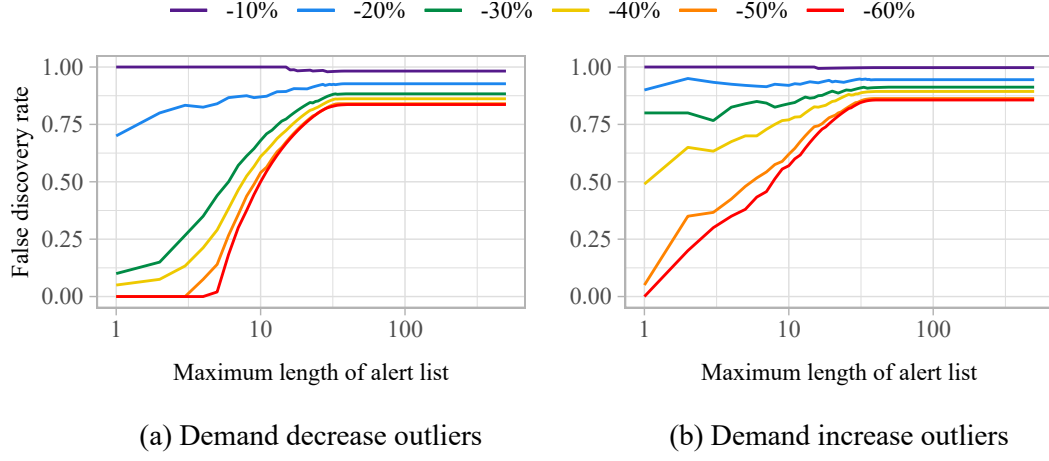


Figure 25: False discovery rate for homogeneous demand-volume outliers by magnitude

C.2.5 Outliers affecting a single itinerary

Figure 26 shows the true positive rate for the remaining itineraries in Figure 14 of Section 4.4.

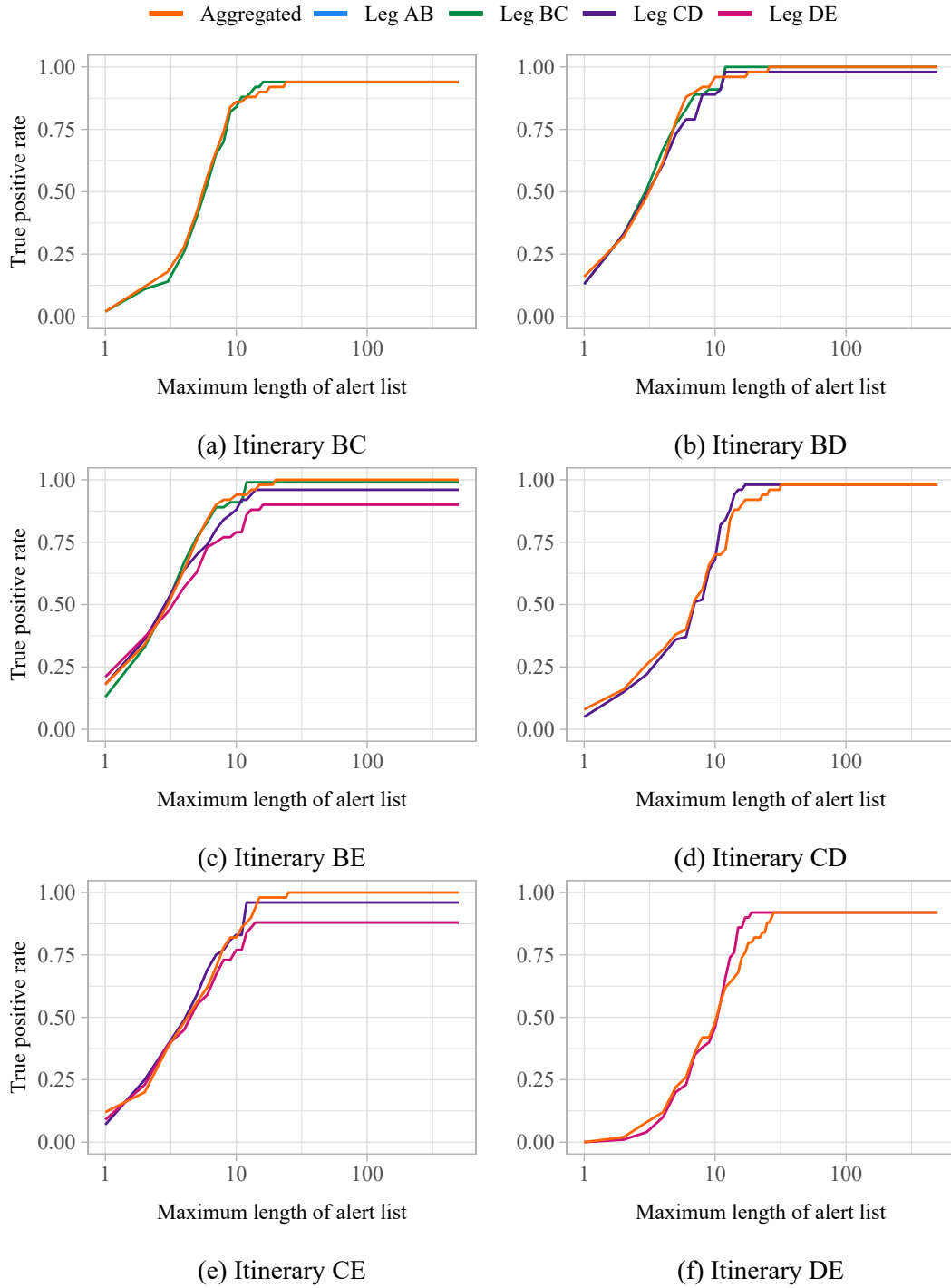


Figure 26: True positive rate for single itinerary outliers (cont.)

C.2.6 Outliers affecting a subset of itineraries

We consider a case where demand outliers affect only a subset of itineraries. Practical examples for this phenomenon could include trade fairs or conventions as well as regional crises. In such situations, demand towards (or from) a specific destination is most affected. Here, clustering offers additional benefits in guiding analysts towards those itineraries where they should adjust the forecast or controls.

We differentiate four scenarios based on the four-leg-network described in Section 4, where events affect demand for itineraries travelling to stations B, C, D, and E respectively. We expect analogous results when customers aim to travel home from events that happened at stations A, B, C, or D respectively, given the symmetry of the demand parameters chosen for the computational study.

For each of the four possible events considered, we investigate the case where this generates 50% increase in average leg demand. For simplicity, we assume these passengers are equally split between the itineraries which alight at the relevant station. Table 8 shows the resulting demand increases for each leg.

| Event at Station | Itineraries Affected | Additional 120 Passengers in Itineraries | | | |
|------------------|----------------------|--|--------------|--------------|-------------|
| | | Resulting Demand Increase per Leg | | | |
| | | Leg AB | Leg BC | Leg CD | Leg DE |
| B | A-B | +120 (+50%) | - | - | - |
| C | A-C, B-C | +60 (+25%) | +120 (+50%) | - | - |
| D | A-D, B-D, C-D | +40 (+16.6%) | +80 (+33.3%) | +120 (+50%) | - |
| E | A-E, B-E, C-E, D-E | +30 (12.5%) | +60 (+25%) | +90 (+37.5%) | +120 (+50%) |

Table 8: Changes in leg demand resulting from an additional 120 passengers in itinerary demand

Figure 27a shows the true positive rate for each of the cases. Although the event at E generates outliers in more legs, it is not the case that it has the highest true positive rate. This shows that though the approach aggregates across legs, it does not ignore outliers only in a subset of those legs, provided they are sufficiently large. These effects may also be caused by interactions between the booking limits on different legs. For example, in the case of an event at C, large increases in demand in legs AB and BC may cause booking limits to be reached earlier for these legs, which also limits bookings in itineraries such as AD and AE. Hence, an increase in demand for some legs may caused a decrease in bookings for different legs. By jointly considering multiple legs for outlier detection, we are able to detect the knock-on effects of outliers even when the change in demand only affects a subset of legs. The change in precision can be interpreted similarly, in Figure 27b.

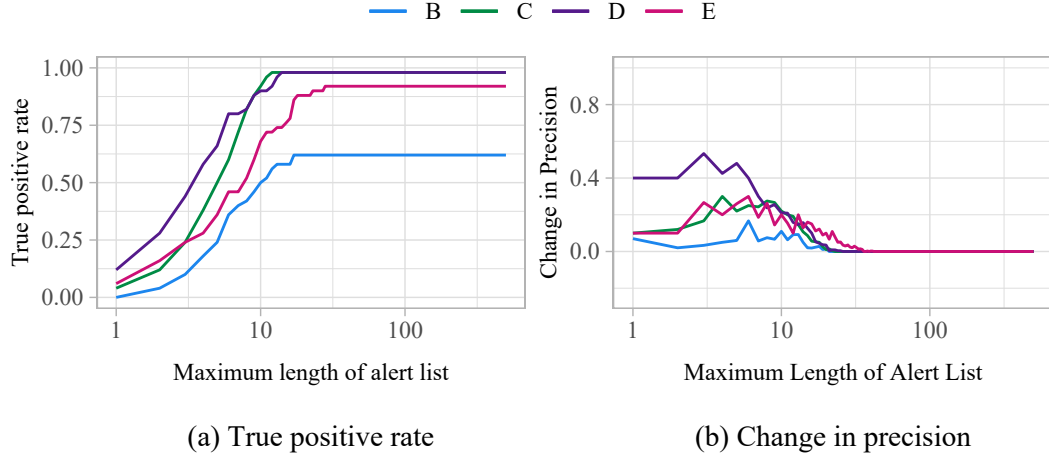


Figure 27: Performance for demand-volume outliers in a subset of itineraries caused by an absolute increase in demand

Had we considered outlier detection on a leg-by-leg basis, the outliers were more likely to be missed in some of the legs. By combining information across legs, we are better able to determine which itineraries are affecting the volume of demand.

C.2.7 Using outlier severity threshold to limit alert list length

The results in this paper focus on limiting the length of the ranked alert list simply by the number of alerts it contains as this is most relevant to analysts. However, an alternative approach limits the length of the list by the outlier severity assigned to each departure. For example, classifying a train as an outlier only if its outlier severity is above 80%.

Detection results when outliers affect all itineraries

Figure 28 shows the true positive rate as the outlier severity decreases from 100% to 0%.

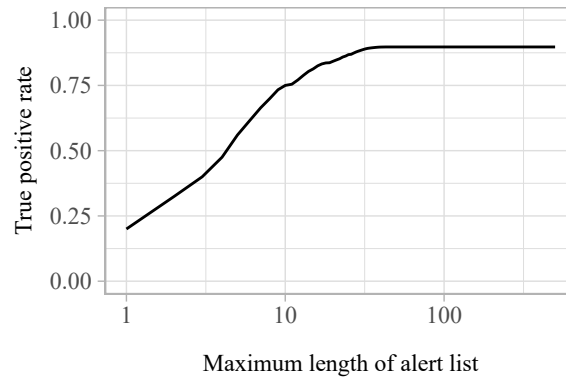


Figure 28: True positive rate for nonhomogeneous demand-volume outliers as minimum outlier severity varies

Results are similar to those shown in Figure 12a. Figure 29 shows the true positive rate as

the outlier severity decreases from 100% to 0%, for each magnitude of outlier considered. Results are similar to those shown in Figure 15.

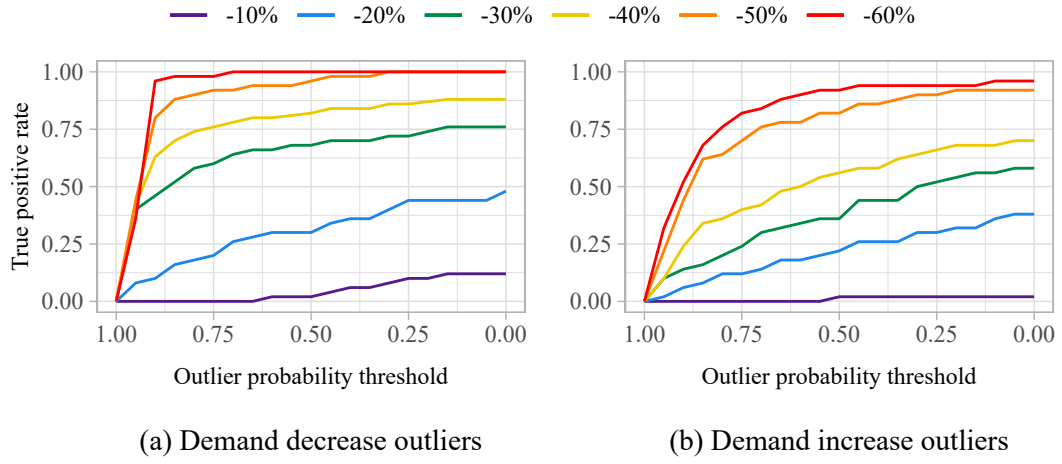


Figure 29: True positive rate for homogeneous demand-volume outliers by magnitude

Detection results when outliers affect a single itinerary

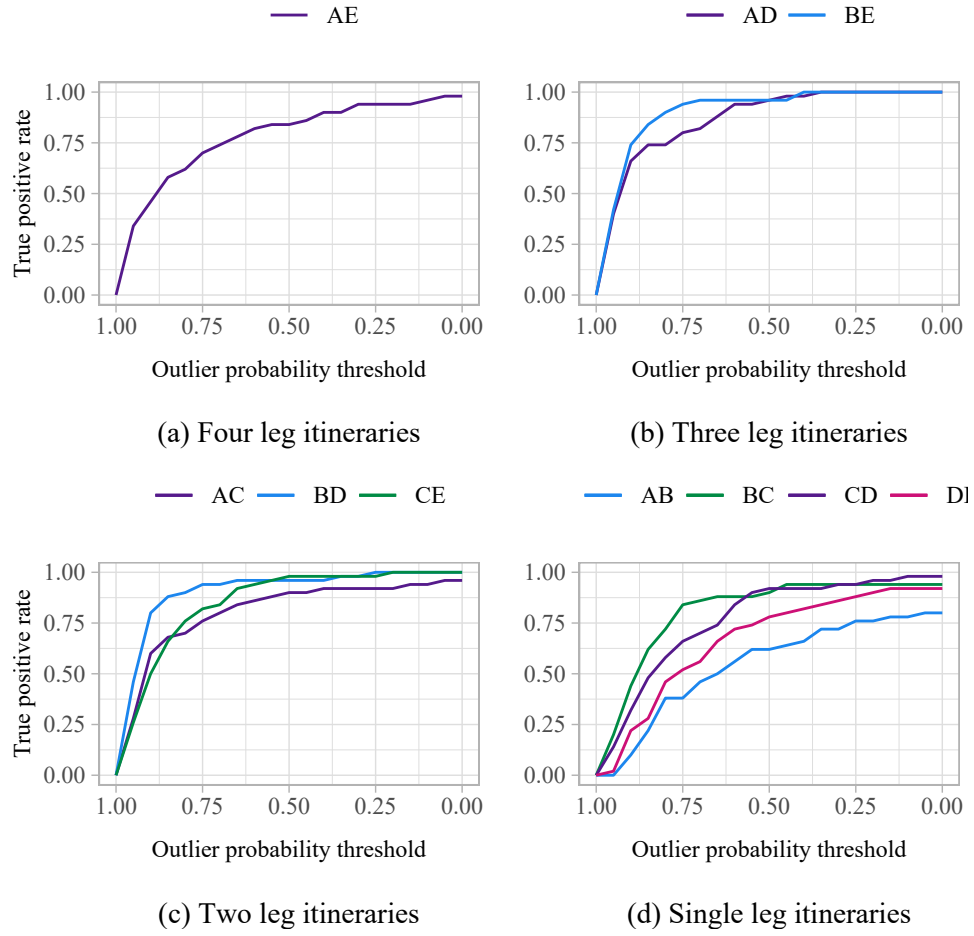


Figure 30: True positive rate for single itinerary demand-volume outliers as minimum outlier severity varies

C.3 Revenue benefits from forecast adjustments for outlier demand

Figure 31 shows the true positive rate for the remaining itineraries in Figure 17 of Section 5.3.

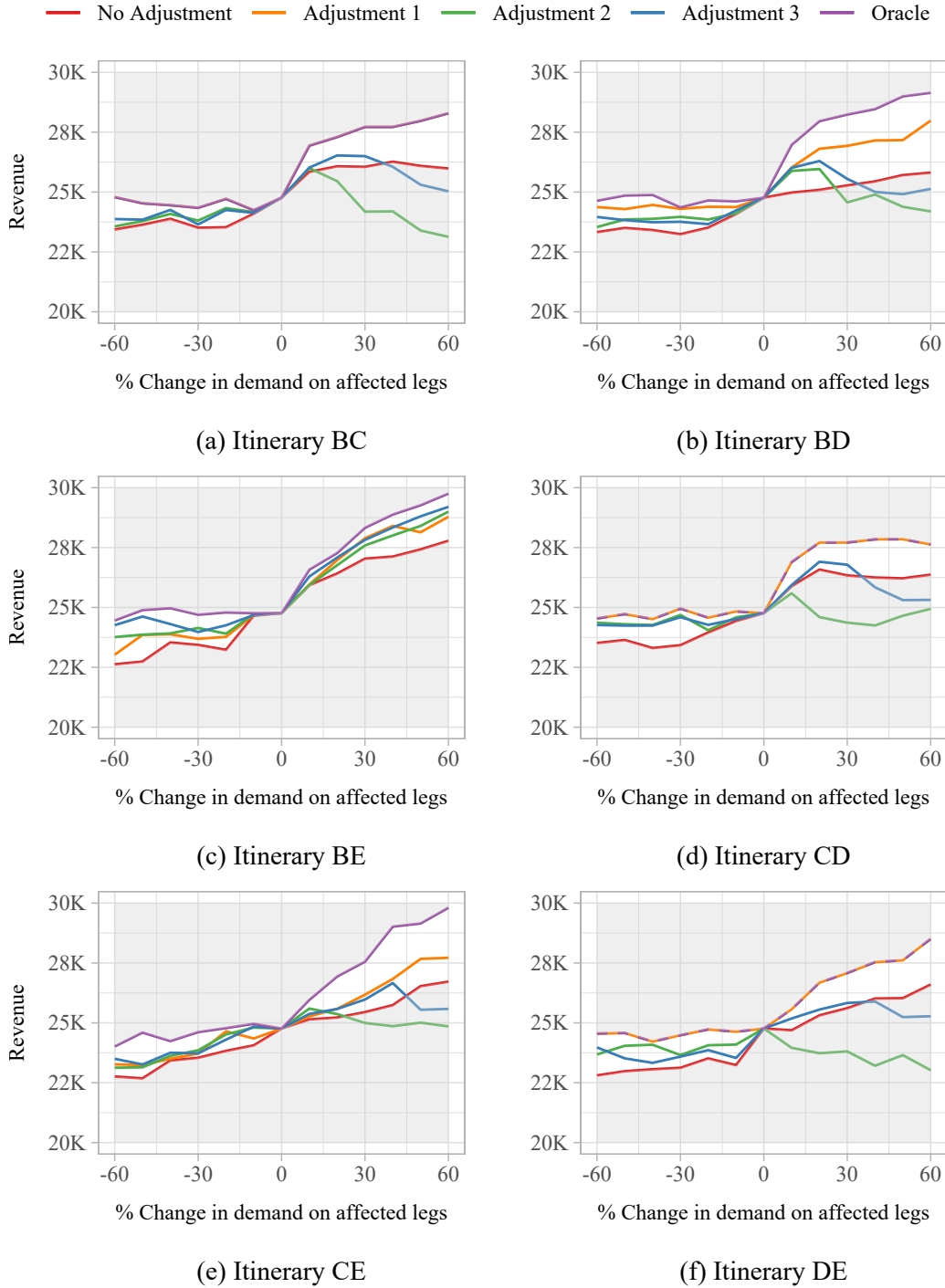


Figure 31: Revenue generated under different itinerary-level forecast adjustments (cont.)

The analysis in Section 5.2 constitutes a best-case scenario in which we assume that, if outlier demand affects a particular leg, the outlier is detected in that leg. However, as we show in Section 4.4, even when demand outliers affect multiple legs, the outlier is not always detected in every leg due to noise. Therefore, we additionally compare different adjustments based on the output of the outlier detection, for an outlier in itinerary AE.

- **Adjustment A:** Adjust only the forecasts of the affected single-leg itineraries for those legs in which the outlier is detected.
- **Adjustment B:** Adjust the forecasts of the affected single-leg itineraries for those legs in which the outlier is detected, **and** the cluster spanning itinerary (AE).

We compare these both to making no adjustment, and to the oracle adjustment. This is still a best-case scenario to some extent, given that we assume the correct magnitude of adjustment is made.

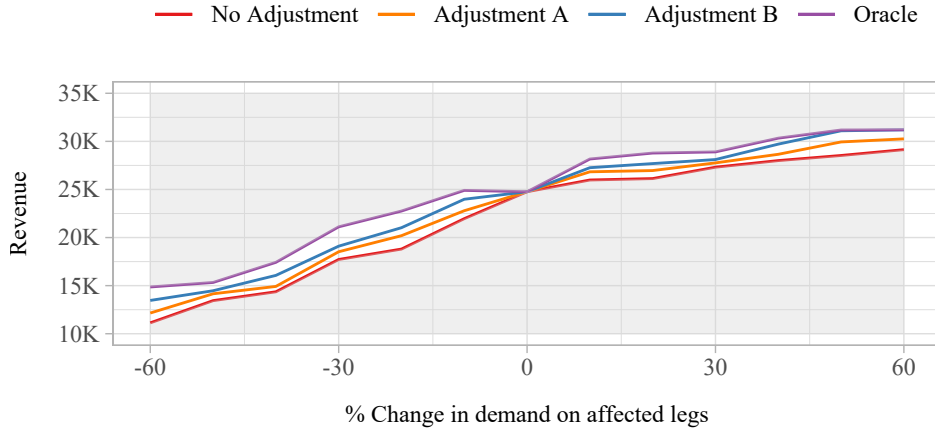


Figure 32: Revenue generated under different forecast adjustments resulting from the outlier detection for outlier demand in itinerary AE

Figure 32 shows the revenue under adjustments A and B (as described in Section 5.2) depending on the output of the outlier detection procedure. Combining adjustments on the leg-level with those on the cluster level provides superior results in contrast to leg level adjustments alone. Though making adjustments to only the single-leg itineraries may be risk averse in the rare cases where an outlier affects only a small subset of the legs within a cluster, it may be detrimental to revenue when outliers affect multiple legs.

D Empirical study of Deutsche Bahn booking data

Appendix D contains additional analysis of the empirical booking data from Deutsche Bahn, as described in Section 3.

D.1 Model selection for functional regression

Due to the functional nature of the data, in order to determine which of the factors result in a better fitting model, we use the **Cross-Validated Sum Of Integrated Squared Errors** (CV-SSE).

$$CV-SSE = \sum_{n=1}^N \int (y_{nl}(t) - \hat{y}_{nl}(t))dt, \quad (42)$$

where $\hat{y}_{nl}(t)$ is the prediction for the n^{th} booking pattern on the leg l , under the model fitted to all but the n^{th} booking pattern. The model which produces the lowest CV-SSE is chosen as the best fitting. Note that unlike other model selection criterion (e.g. AIC), CV-SSE does not take into account the number of parameters. Given that we are not interested in out of sample prediction, only in obtaining the best fitting model for our data, over-fitting is not of great concern. The values of the CV-SSE for each of the 12 models considered are shown in Table 9.

| Model | Intercept | Day | Month | Short Horizon (I) | Short Horizon (C) | CV-SSE | | | |
|----------|-----------|-----|-------|----------------------|----------------------|-----------------|-----------------|-----------------|-----------------|
| | | | | | | Leg AB | Leg BC | Leg CD | Leg DE |
| Model 1 | ✓ | | | | | 79974160 | 75034839 | 79529280 | 73824611 |
| Model 2 | ✓ | | | ✓ | | 58617546 | 52622148 | 52424683 | 50009080 |
| Model 3 | ✓ | | | | ✓ | 58620898 | 52863263 | 52506946 | 50014984 |
| Model 4 | ✓ | ✓ | | | | 27227350 | 35376732 | 32789181 | 30037659 |
| Model 5 | ✓ | ✓ | | ✓ | | 26551341 | 33724380 | 32282900 | 29989390 |
| Model 6 | ✓ | ✓ | | | ✓ | 26704943 | 34154782 | 32439972 | 30019196 |
| Model 7 | ✓ | | ✓ | | | 58620649 | 57895619 | 52638923 | 50015645 |
| Model 8 | ✓ | | ✓ | ✓ | | 58608640 | 57865403 | 52615801 | 49996331 |
| Model 9 | ✓ | | ✓ | | ✓ | 58878374 | 57885484 | 52654330 | 50033157 |
| Model 10 | ✓ | ✓ | ✓ | | | 24574978 | 25700166 | 21691111 | 21880038 |
| Model 11 | ✓ | ✓ | ✓ | ✓ | | 24519539 | 25691637 | 21689686 | 21878259 |
| Model 12 | ✓ | ✓ | ✓ | | ✓ | 24546715 | 25697938 | 21724073 | 21896889 |

Table 9: Model comparison for functional regression

Across all legs, we find that day, month, and shortened booking horizons are all factors that must be taken into account. The inclusion of the days of the week as factors significantly reduces the CV-SSE. In comparison, the inclusion of the booking horizon variable has a smaller, though still positive, effect. We compare two different approaches to accounting for the shortened booking horizon: (i) an indicator function (I) equal to 1 if the booking horizon is shorter, and (ii) a continuous variable (C) between 0 and 1 which gives the length of the shortened horizon as a proportion of the regular length horizon. Based on the CV-SSE scores, shortened booking horizons are best represented

by the indicator function i.e. it is important to know that it is shorter but not by how much. The smaller effect of the horizon length variable may be related to the inclusion of the month variable, which is unsurprising given the overlap in the definition of these variables. The values of the CV-SSE is similar for the models 2 and 7, where we only consider one of month or horizon length as a factor.

D.2 Residual booking patterns

Figure 33 shows the residual booking patterns resulting from the functional regression applied in equation (7) of Section 3.2. Compare with Figure 8 of Section 3.2 – the obvious outliers are preserved.

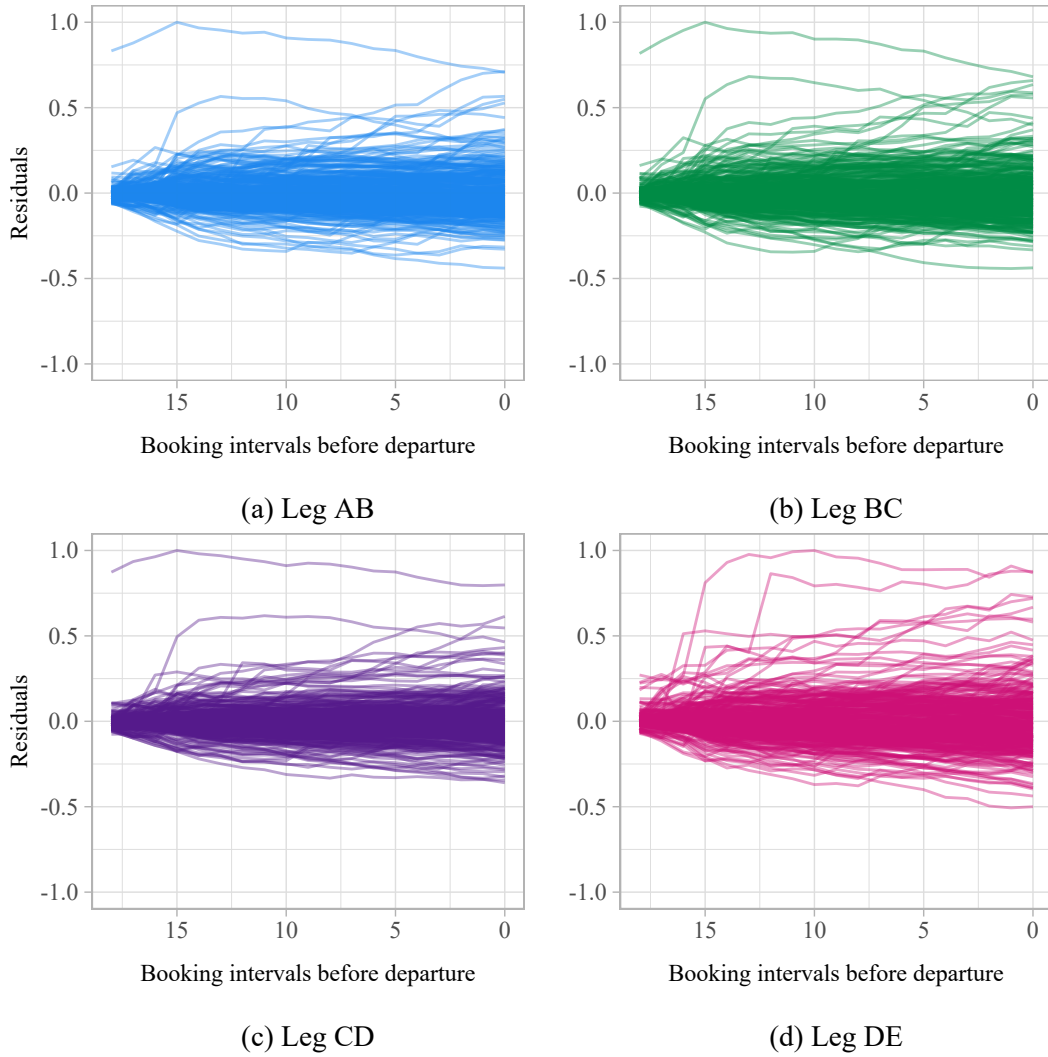


Figure 33: Residual booking patterns

D.3 Functional linear regression coefficients

Table 10 shows an example of the coefficients for each explanatory variable over the 19 booking intervals, along with their standard errors. Not all days of the week, or months of the year, are significant throughout the entire booking horizon. Similarly, some days of the week have much stronger significance than others e.g. Saturdays have a much larger impact than Tuesdays.

| Coefficient | t = 1 | 2 | 3 | 4 | 5 | 6 | 7 | 8 | 9 |
|-------------------------|------------|------------|------------|------------|------------|------------|------------|------------|------------|
| β_{0t} | 1.4 (1.0) | 1.8 (1.1) | 5.4 (1.2) | 11.2 (1.4) | 13.8 (1.5) | 14.8 (1.5) | 15.2 (1.6) | 16.4 (1.6) | 17.7 (1.6) |
| β_{1t} [Mon] | -0.4 (0.8) | -1.0 (0.9) | -1.5 (1.0) | -2.1 (1.2) | -1.6 (1.2) | -0.7 (1.3) | -0.1 (1.3) | 0.5 (1.4) | 0.8 (1.4) |
| β_{2t} [Tue] | -1.2 (0.8) | -2.1 (0.9) | -3.7 (1.0) | -5.1 (1.2) | -5.8 (1.2) | -6.3 (1.3) | -6.8 (1.2) | -6.4 (1.3) | -6.4 (1.4) |
| β_{3t} [Wed] | -1.2 (0.8) | -1.9 (0.9) | -3.9 (1.0) | -5.2 (1.2) | -6.5 (1.2) | -7.1 (1.3) | -7.3 (1.3) | -7.4 (1.3) | -8.9 (1.4) |
| β_{4t} [Thu] | -1.0 (0.8) | -1.3 (0.9) | -3.2 (1.0) | -4.3 (1.2) | -5.6 (1.2) | -6.7 (1.3) | -6.7 (1.3) | -7.1 (1.3) | -7.8 (1.4) |
| β_{5t} [Fri] | -0.5 (0.8) | -0.4 (0.9) | -0.7 (1.0) | -0.3 (1.2) | 0.8 (1.2) | 1.5 (1.3) | 2.6 (1.3) | 2.7 (1.4) | 2.9 (1.4) |
| β_{6t} [Sat] | 5.5 (0.8) | 10.9 (0.9) | 17.1 (1.1) | 25.5 (1.2) | 30.4 (1.3) | 33.5 (1.3) | 36.9 (1.3) | 38.6 (1.4) | 41.2 (1.4) |
| β_{7t} [Jan] | -0.7 (0.9) | -0.3 (1.0) | -1.3 (1.2) | -4.3 (1.3) | -5.0 (1.4) | -4.8 (1.5) | -4.5 (1.5) | -5.0 (1.5) | -4.4 (1.6) |
| β_{8t} [Feb] | 0.3 (1.0) | 1.8 (1.1) | 0.0 (1.3) | -4.0 (1.4) | -3.5 (1.5) | -2.3 (1.6) | -0.3 (1.6) | 0.3 (1.7) | 1.6 (1.7) |
| β_{9t} [Mar] | 0.2 (1.0) | 0.9 (1.1) | 0.4 (1.2) | -3.2 (1.4) | -4.4 (1.5) | -4.0 (1.6) | -3.2 (1.6) | -2.9 (1.7) | -2.5 (1.7) |
| β_{10t} [Apr] | 0.3 (1.0) | 2.1 (1.1) | 1.2 (1.3) | 0.9 (1.4) | 3.1 (1.5) | 4.8 (1.6) | 5.6 (1.6) | 5.6 (1.7) | 5.9 (1.7) |
| β_{11t} [May] | 3.5 (1.0) | 4.4 (1.1) | 4.1 (1.2) | 0.7 (1.4) | -0.1 (1.5) | 0.0 (1.6) | 0.6 (1.6) | 0.5 (1.7) | 0.9 (1.7) |
| β_{12t} [Jun] | 0.2 (1.0) | 1.9 (1.1) | 0.7 (1.3) | -1.9 (1.4) | -2.6 (1.5) | -2.2 (1.6) | -1.9 (1.6) | -2.0 (1.7) | -1.5 (1.7) |
| β_{13t} [Jul] | 0.4 (0.8) | 1.6 (1.1) | 1.4 (1.2) | -1.5 (1.4) | -1.8 (1.5) | -0.7 (1.6) | -0.3 (1.6) | 0.1 (1.7) | 0.9 (1.7) |
| β_{14t} [Aug] | 1.5 (1.0) | 3.3 (1.1) | 3.3 (1.3) | 3.7 (1.5) | 5.0 (1.6) | 6.4 (1.6) | 7.7 (1.7) | 8.3 (1.7) | 9.8 (1.7) |
| β_{15t} [Sep] | 1.9 (1.1) | 2.5 (1.2) | 2.1 (1.3) | -1.2 (1.5) | -0.7 (1.6) | 0.6 (1.6) | 1.5 (1.7) | 2.3 (1.7) | 3.5 (1.8) |
| β_{16t} [Oct] | 1.6 (1.0) | 3.5 (1.1) | 3.8 (1.2) | 4.7 (1.4) | 7.0 (1.5) | 8.8 (1.6) | 11.2 (1.6) | 12.6 (1.7) | 15.5 (1.7) |
| β_{17t} [Nov] | 1.0 (0.9) | 2.8 (1.1) | 4.2 (1.3) | 4.5 (1.4) | 6.7 (1.5) | 9.3 (1.6) | 11.0 (1.6) | 11.5 (1.7) | 12.5 (1.7) |
| β_{18t} [Horizon] | -1.2 (0.9) | -0.2 (1.0) | 0.7 (1.2) | -0.8 (1.3) | -1.1 (1.4) | -0.6 (1.5) | -0.5 (1.5) | -0.2 (1.5) | -0.4 (1.6) |

| t = 10 | 11 | 12 | 13 | 14 | 15 | 16 | 17 | 18 | 19 |
|------------|------------|------------|-------------|-------------|-------------|-------------|-------------|-------------|-------------|
| 18.5 (1.7) | 18.7 (1.7) | 19.5 (1.7) | 20.7 (1.8) | 22.2 (1.8) | 24.1 (1.8) | 26.0 (1.8) | 27.9 (1.9) | 29.0 (1.9) | 30.4 (2.0) |
| 1.1 (1.4) | 1.1 (1.4) | 1.1 (1.5) | 0.4 (1.5) | -0.6 (1.5) | -1.1 (1.5) | -2.5 (1.6) | -3.7 (1.6) | -3.5 (1.6) | -2.1 (1.7) |
| -6.8 (1.4) | -5.8 (1.4) | -5.7 (1.5) | -6.4 (1.5) | -7.4 (1.5) | -8.0 (1.5) | -9.3 (1.6) | -10.2 (1.6) | -10.0 (1.6) | -9.1 (1.6) |
| -9.2 (1.4) | -8.9 (1.4) | -9.1 (1.5) | -10.0 (1.5) | -11.2 (1.5) | -12.7 (1.5) | -14.5 (1.6) | -14.7 (1.6) | -15.1 (1.6) | -15.2 (1.7) |
| -7.8 (1.4) | -7.6 (1.4) | -7.7 (1.5) | -8.9 (1.5) | -10.7 (1.5) | -12.1 (1.5) | -12.9 (1.6) | -13.6 (1.6) | -13.7 (1.6) | -13.7 (1.7) |
| 4.2 (1.4) | 5.0 (1.4) | 5.4 (1.5) | 4.3 (1.5) | 4.0 (1.5) | 4.6 (1.5) | 5.0 (1.6) | 5.8 (1.6) | 6.4 (1.6) | 7.1 (1.7) |
| 45.0 (1.4) | 46.1 (1.5) | 48.1 (1.5) | 49.4 (1.5) | 50.7 (1.5) | 53.1 (1.6) | 55.1 (1.6) | 57.1 (1.6) | 58.5 (1.7) | 59.4 (1.7) |
| -3.7 (1.6) | -3.0 (1.7) | -3.8 (1.7) | -3.6 (1.7) | -3.1 (1.7) | -3.5 (1.8) | -3.3 (1.8) | -3.8 (1.8) | -3.1 (1.9) | -3.8 (1.9) |
| 3.3 (1.8) | 3.7 (1.8) | 3.9 (1.8) | 4.9 (1.8) | 5.9 (1.9) | 6.8 (1.9) | 7.8 (1.9) | 8.2 (2.0) | 9.5 (2.0) | 9.2 (2.1) |
| -1.6 (1.7) | -0.8 (1.8) | -1.1 (1.8) | -0.6 (1.8) | -0.2 (1.9) | -0.6 (1.9) | -0.4 (1.9) | -0.8 (2.0) | -0.3 (2.0) | -0.7 (2.0) |
| 6.1 (1.8) | 6.3 (1.8) | 6.3 (1.8) | 6.8 (1.8) | 7.2 (1.9) | 7.3 (1.9) | 7.2 (1.9) | 7.1 (2.0) | 8.3 (2.0) | 8.8 (2.0) |
| 1.1 (1.7) | 1.4 (1.8) | 1.3 (1.8) | 1.8 (1.8) | 2.5 (1.9) | 2.3 (1.9) | 2.4 (1.9) | 2.1 (2.0) | 3.1 (2.0) | 3.5 (2.0) |
| -1.0 (1.8) | -0.4 (1.8) | -0.2 (1.8) | 0.9 (1.8) | 1.5 (1.9) | 1.1 (1.9) | 1.1 (1.9) | 0.7 (2.0) | 2.0 (2.0) | 2.9 (2.0) |
| 1.8 (1.7) | 2.5 (1.8) | 2.6 (1.8) | 3.1 (1.8) | 4.0 (1.9) | 4.0 (1.9) | 4.4 (1.9) | 4.6 (2.0) | 6.3 (2.0) | 6.9 (2.0) |
| 11.6 (1.8) | 12.8 (1.8) | 13.2 (1.8) | 14.0 (1.9) | 15.4 (1.9) | 16.4 (1.9) | 17.1 (2) | 17.4 (2.0) | 19.2 (2.1) | 21.7 (2.1) |
| 5.1 (1.8) | 6.8 (1.8) | 7.3 (1.9) | 8.7 (1.9) | 9.9 (1.9) | 10.2 (2.0) | 11.6 (2.0) | 11.6 (2.0) | 12.4 (2.1) | 13.3 (2.1) |
| 17.0 (1.7) | 18.4 (1.8) | 19.2 (1.8) | 20.7 (1.8) | 22.0 (1.9) | 22.9 (1.9) | 24.6 (1.9) | 25.3 (2.0) | 27.6 (2.0) | 28.0 (2.0) |
| 13.4 (1.8) | 14.0 (1.8) | 14.0 (1.8) | 15.1 (1.8) | 15.8 (1.9) | 15.9 (1.9) | 16.2 (1.9) | 16.1 (2.0) | 16.6 (2.0) | 16.2 (2.0) |
| -0.2 (1.6) | 0.2 (1.7) | 1.2 (1.7) | 1.9 (1.7) | 2.6 (1.7) | 2.9 (1.8) | 3.2 (1.8) | 4.5 (1.8) | 5.4 (1.9) | 6.0 (1.9) |

Table 10: Functional linear regression coefficients (and standard errors)

D.4 Functional depths

Figure 34 shows the functional depths for the empirical residual booking patterns, before the functional depths are transformed into the z_{nl} , as shown in Figure 9 of Section 3.2.

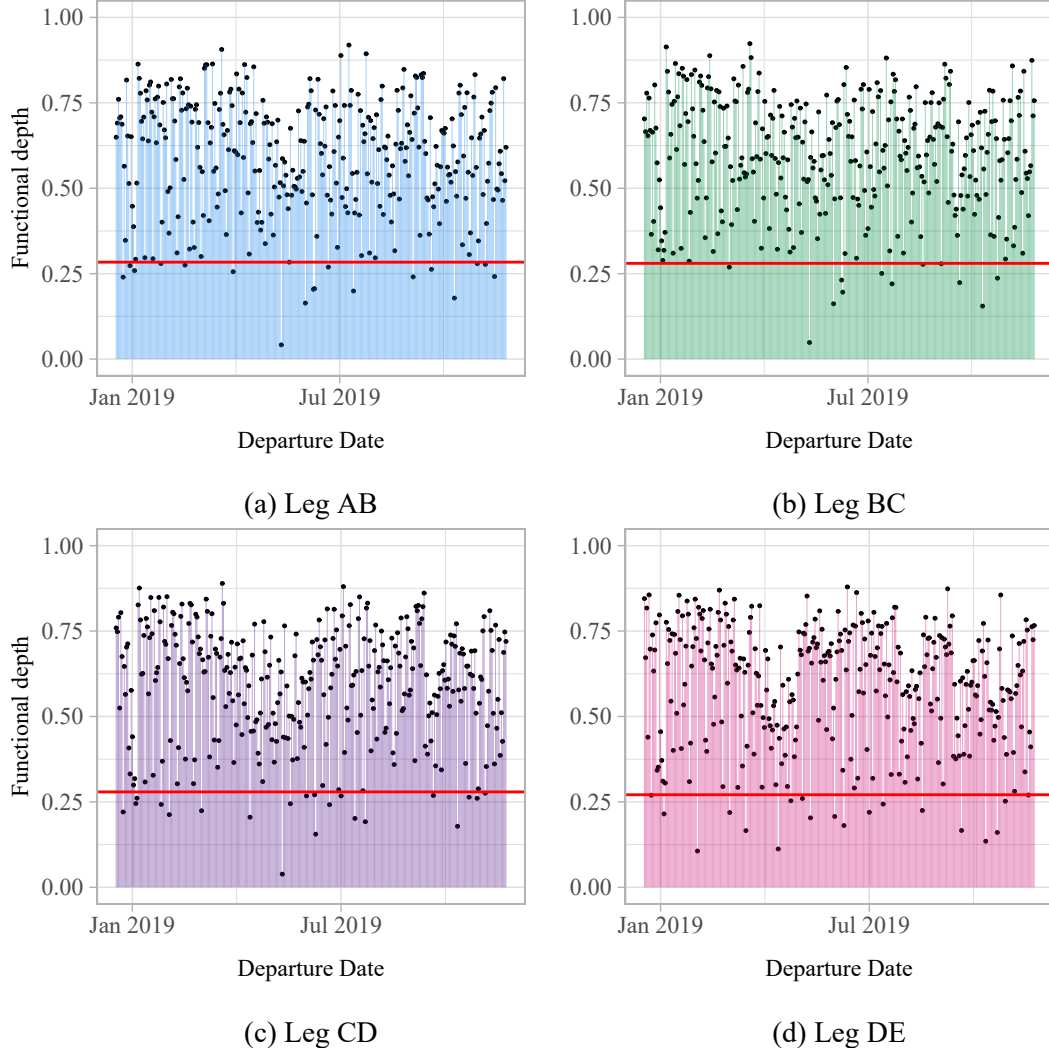


Figure 34: Functional depths

D.5 Probability plots for GPD and Exponential distributions

Given that, if both $\mu = 0$ and $\xi = 0$, the GPD reduces to an exponential distribution, it is appropriate to compare the fit of the GPD with an exponential distribution to check if the inclusion of additional parameters is beneficial. Figure 35 shows the P-P plots, i.e. the fitted theoretical CDF against the empirical CDF for the GPD (Figure 35a) and the Exponential distribution (Figure 35b). The GPD provides a closer fit to the empirical data and the additional parameters better account for the shape of the distribution. The GPD does not provide a perfect fit, with the probabilities in the bottom

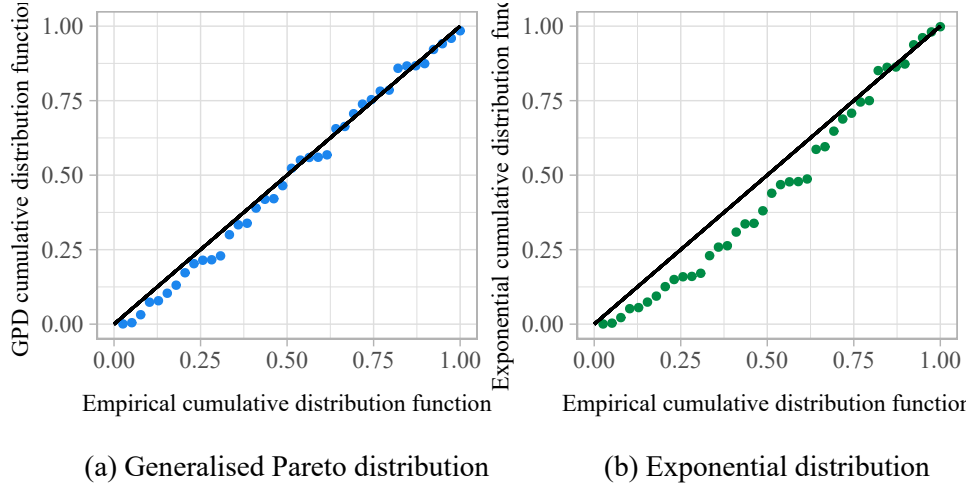


Figure 35: P-P plots

left of Figure 35a on consistently being underestimated. However, given that we assume points with very low probability are more likely to be false positives, under-estimating may actually be beneficial. Further, only the highly-ranked outliers i.e. those with high probability, are likely to be considered by an analyst due to time-constraints. The GPD provides a very good fit for those data points. If there is a sufficiently large number of threshold exceedances, an empirical distribution could alternatively be used to compute the probabilities.

D.6 Distribution of outliers across multiple legs

The proportion of outliers found in each number of legs is shown in Figure 36, with over half of the outliers detected in multiple legs. Compared with Figure 22, this shows a similar proportion of outliers as found in the simulation study.

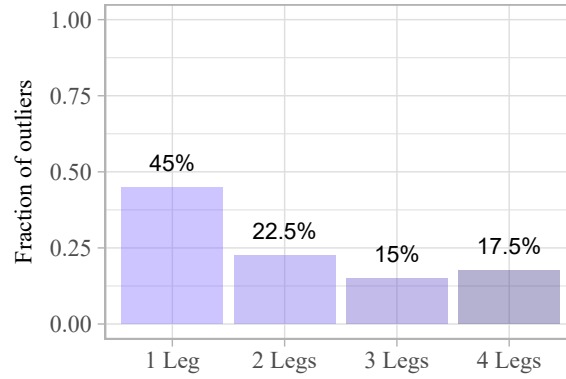


Figure 36: Fraction of all outliers detected in 1, 2, 3, or 4 legs

Figure 37a shows the proportion of total outlying booking patterns in terms of which legs they were detected as outliers in. Figure 37b shows the proportion in each leg of outlying booking patterns detected in one leg only. The proportions are fairly evenly split between the different legs. This reassures us that the correct clustering was chosen - if leg DE did in fact belong to a separate second cluster, we would expect a higher proportion of single leg outliers to have been found in leg DE – compare with Figure 23.

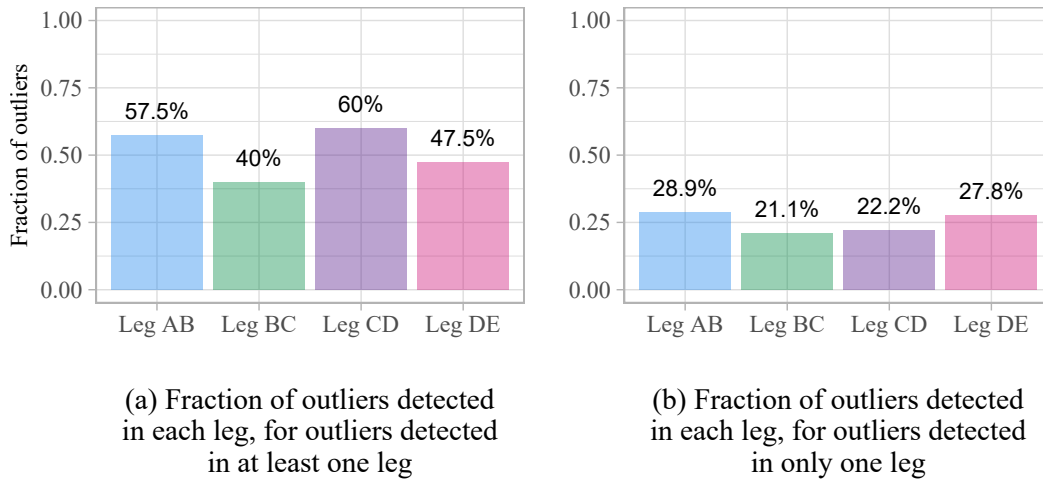


Figure 37: Fraction of outliers detected in each leg

D.7 Simulation verification

In order to validate the parameter choices used to simulate booking patterns, we compare the resulting simulated booking patterns with the empirical booking patterns. We

consider the standard deviation and mean of the bookings across the booking horizon of each in Figure 38. Both the empirical and simulated booking patterns show a similar shape and magnitude of relationship between the mean and standard deviation across the booking horizon.

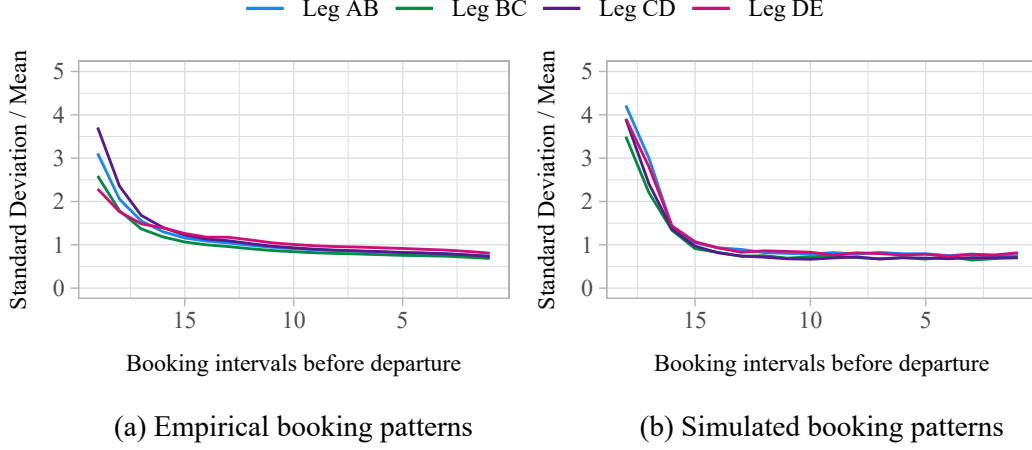


Figure 38: Comparison of standard deviation divided by mean of booking patterns

We also compare the correlations between the different legs for both the empirical and simulated data. Table 11 shows the functional dynamical correlation between the empirical booking patterns, and empirical residual booking patterns, for each leg. Table 12 shows the corresponding correlations between the simulated booking patterns. The values are similar and the rate of decay between legs as they get further apart follows a similar pattern.

| | Leg AB | Leg BC | Leg CD | Leg DE |
|--------|--------|--------|--------|--------|
| Leg AB | - | 0.95 | 0.83 | 0.70 |
| Leg BC | - | - | 0.83 | 0.66 |
| Leg CD | - | - | - | 0.78 |
| Leg DE | - | - | - | - |

(a) Booking patterns

| | Leg AB | Leg BC | Leg CD | Leg DE |
|--------|--------|--------|--------|--------|
| Leg AB | - | 0.92 | 0.75 | 0.58 |
| Leg BC | - | - | 0.88 | 0.74 |
| Leg CD | - | - | - | 0.84 |
| Leg DE | - | - | - | - |

(b) Residual booking patterns

Table 11: Functional dynamical correlation of empirical booking patterns

| | Leg AB | Leg BC | Leg CD | Leg DE |
|--------|--------|--------|--------|--------|
| Leg AB | - | 0.81 | 0.72 | 0.60 |
| Leg BC | - | - | 0.86 | 0.68 |
| Leg CD | - | - | - | 0.78 |
| Leg DE | - | - | - | - |

Table 12: Functional dynamical correlation of simulated booking patterns